Numerical Investigation of the Hydraulic Fracturing Mechanisms in Oil Sands

Siavash Taghipoor[1, 2], Morteza Roostaei[1, 3], Arian Velayati[1], Atena Sharbatian[3], Dave Chan[1] and Alireza Nouri[1]

[1]Department of Civil and Environmental Engineering, University of Alberta, Canada
[2]KGHM International, Canada
[3]RGL Reservoir Management Inc., Canada

Abstract

This paper presents a numerical investigation of hydraulic fracturing in oil sands during cold water injection by considering the aspects of both geomechanics and reservoir fluid flow. According to previous studies, the low shear strengths of unconsolidated or weakly consolidated sandstone reservoirs significantly influence the hydraulic fracturing process. Therefore, classical hydraulic fracture models cannot simulate the fracturing process in weak sandstone reservoirs. In the current numerical models, the direction of a tensile fracture is predetermined based on in situ stress conditions. Additionally, the potential transformation of a shear fracture into a tensile fracture and the potential reorientation of a tensile fracture owing to shear banding at the fracture tip have not yet been addressed in the literature. In this study, a smeared fracture technique is employed to simulate tensile and shear fractures in oil sands. The model used combines many important fracture features, which include the matrix flow, poroelasticity and plasticity modeling, saturation-dependent permeability, gradual degradation of the oil sands as a result of dilative shear deformation, and the tensile fracturing and shear failure that occur with the simultaneous enhancement of permeability. Furthermore, sensitivity analyses are also performed with respect to the reservoir and geomechanical parameters, including the apparent tensile strength and cohesion of the oil sands, magnitude of the minimum and maximum principal stress, absolute permeability and elastic modulus of the oil sands and ramp-up time. All these analyses are performed to clarify the influences of these parameters on the fracturing response of the oil sands.

Keywords

Smeared Fracture; Hydraulic Fracturing; Numerical Simulation, Oil Sand

1 Introduction

Hydraulic fracturing techniques have commonly been used to stimulate hard-rock reservoirs, which typically behave like brittle, linearly elastic materials. These reservoirs are mostly impermeable or exhibit low permeabilities (Xu, 2010). Recently, there has been interest in stimulating unconsolidated and poorly consolidated formations using hydraulic fracturing, wherein the material to be fractured possesses a low shear strength and high permeability (Khodaverdian et al., 2010). In this case, the assumptions of linear elastic fracture mechanics and a small fluid leak-off from the fracture walls may not be valid.

Researchers have found that the mode of failure during the hydraulic fracturing of weakly consolidated sandstone is influenced by material properties such as the dilative behavior, strength, porosity, and permeability of the material, as well as the injection pressure ramp-up rate, injection rate, in situ stresses, injection fluid properties, and possible solid concentrations in the injection fluid (Golovin et al., 2010). Moreover, the wellbore orientation and completion type (e.g., the number and direction of the perforations) can affect the fracture geometry and propagation pattern (Daneshy, 2003, 2011). As a result, a complex fracture zone rather than a simple planar fracture may develop in weakly consolidated sandstones (Daneshy, 2003, 2011).

Based on laboratory hydraulic fracturing experiments on cohesionless sand and weak sandstones, the fracturing mechanisms in these materials are most likely shear failure, tensile failure, or a combination of both (Pak, 1997; Khodaverdian and McElfresh, 2000; Chang, 2004; Bohloli and de Pater, 2006; de Pater and Dong, 2007; Golovin et al., 2010; Jasarevic et al., 2010; Khodaverdian et al., 2010; Zhou et al., 2010; Olson et al., 2011). In addition, field observations indicate that in weak sandstone formations, the hydraulic fractures differ from two-wing planar fractures (Mahrer et al., 1996). Classical models are incapable of describing some of the field observations (Settari, 1988; Weijers et al., 2000; Daneshy, 2003; Onaisi et al., 2011), wherein higher-than-expected fracturing pressures (Papanastasiou, 1997a) or smaller lengths and larger widths of the field fractures are obtained compared to the predictions made using existing numerical models (Settari, 1988; Weijers et al., 2000; Daneshy, 2003). Laboratory experiments have shown that the hydraulic fracturing of weakly/unconsolidated sandstone could develop in the form of shear failures/fractures, tensile fractures, or a combination of these two modes (Daneshy, 2003). The hydraulic conductivity of a tensile fracture is a nonlinear function of the fracture width (Zimmerman and Bodvarsson, 1996; Waite et al., 1999; White, 2011). In shear failure, the permeability of the structure is enhanced owing to dilation and the formation of shear bands (Touhidi-Baghini, 1998). The shear dilation increases the local stresses and consequently increases the fracturing pressure (Pak, 1997). Due to the low strengths of weakly consolidated sandstones, shear failure/fracturing of the reservoir rock during injection is likely to occur. This has been related to phenomena such as multiple fracturing and fracture branching, which have been observed in field operations (Daneshy, 2003), which are generally neglected in numerical hydraulic fracture models.

Many researchers have conducted theoretical and experimental investigations of the initiation and subsequent propagation of tensile fractures (Hagoort et al., 1980; Settari, 1980; Nghiem et al., 1984; Papanastasiou, 1997b; van Dam et al., 2000; Wu, 2006; Ji, 2008). These studies assumed that a two-wing planar fracture occurs parallel to the minimum principal stress. This assumption, however, may not result in realistic outcomes and may also yield misleading results (Di Lullo et al., 2004) when shear fracturing occurs (Di Lullo et al., 2004; Bohloli and de Pater, 2006; Huang et al., 2011).

Recently presented hydraulic fracture models, especially those that are based on the discrete fracture method, assume a two-wing planar fracture, which is typically observed in strong rocks. Weakly consolidated sand formations have been found to be vulnerable to compressive failure across the water injection wells, thereby resulting in shear dilation, as has been shown in many experiments (Khodaverdian and McElfresh, 2000; McElfresh et al., 2002; Di Lullo et al., 2004; Daneshy, 2003 and 2011; Bohloli and de Pater, 2006; Golovin et al., 2010). Increased permeabilities and shear stresses can be formed because of shear dilation. Planar tensile fractures commonly occur in competent rocks; however, shear failure may result in the formation of a fracture network (Pak, 1997; Pak and Chan, 2004; Zhai, 2006; Xu and Wong, 2010). A two-wing tensile fracture with a defined fracture orientation may not be an accurate assumption for the simulation of hydraulic fracturing in weakly consolidated sandstones, as discussed in literature. Therefore, new modeling methods should be developed to obtain more accurate results. Other continuum-based numerical models require a predetermined fracture direction (e.g. Ji, 2008). Although some recent continuum models have been developed to simulate fractures in general directions (e.g. Xu, 2010), they lack a proper tensile fracture-flow law, or they do not simulate the development of shear bands and their interactions with tensile fractures. Models have been developed by using discontinuum mechanics in the form of the discrete element method (DEM) and other methods. These models, however, are computationally costly and impractical for large-scale field problems.

A numerical hydraulic fracturing model for weak rocks should accurately simulate various possible failure modes and their interactions. The smeared fracture modeling approach is believed to be capable of simulating the potential mechanisms that occur in the hydraulic fracturing of cohesionless sands and weakly consolidated sandstones. Current smeared fracturing models used for hydraulic fracturing simulations have certain limitations, such as the inability to distinguish between the flow conductivity of a shear failure/fracture and a tensile fracture (Xu, 2010). Additionally, they may designate a constant permeability to the tensile fractures, which is independent from the fracture aperture (Zhai, 2006). Fluid flow physics differs between compressive and tensile fractures. In tensile fractures, fluid flow can be considered as flow through a clean and infinitely conductive fluid domain, whereas flow in shear fractures can be assumed to be flow through crushed materials. The parallel-plate theory can be used to model the

fluid flow through a tensile fracture. Under such conditions, the hydraulic conductivity of the fracture depends on the aperture of the fracture. The permeability of crushed rocks in the fracture band is affected by the fabric changes and dilative deformation of the shear bands in shear fractures. Current smeared fracture models only incorporate diffused shear failure regions.

In this study, a pseudo three-dimensional numerical tool was developed to simulate hydraulic fracturing in weakly consolidated sandstones. The model is capable of simulating the possible failure modes and fracture rotation around injection wellbores. The model was validated using a field dataset that was obtained via well tests in oil sands.

2 Review of Numerical Hydraulic Fracturing Models

Tensile-mode hydraulic fracturing has been extensively studied over the past decades (Pak, 1997; Papanastasiou, 1997b; van Dam et al., 2000; Settari et al., 2002b; Cook et al., 2004; Lian et al., 2006; Xue et al., 2006; Ji, 2008; Zandi et al., 2010; Zhang et al., 2010). Several studies have also investigated the shear-mode hydraulic fracturing of weakly consolidated sand (Settari et al., 1989; Pak, 1997; Pak and Chan, 2004; Zhai and Sharma, 2005; Wu, 2006; Zhai, 2006; Xu, 2010; Xu and Wong, 2010).

The assumptions of linear elastic fracture mechanics (LEFM) for crack-tip propagation and a tensile two-wing fracture are not valid in unconsolidated and weakly consolidated sandstones when plastic deformation is involved (Khodaverdian and McElfresh, 2000; McElfresh et al., 2002; Di Lullo et al., 2004; Bohloli and de Pater, 2006; Huang et al., 2011).

The existing numerical hydraulic fracture models are based either on smeared fracturing (Roostaei et al., 2019, Wei & Chen; 2018; Chin and Montgomery, 2004; Zhai and Sharma, 2005; Zhai, 2006; Xu, 2010; Xu and Wong, 2010; Xu et al., 2010), discrete fracturing (Hagoort et al., 1980; Settari, 1980; Nghiem et al., 1984; Settari, 1988; Settari et al., 1989; Settari et al., 1990; Settari et al., 1992; Papanastasiou, 1997a; Papanastasiou, 1997b; Papanastasiou, 1999; van Dam et al., 2000; Settari et al., 2002a, 2002b; Ji et al., 2004, 2006; Wu, 2006; Ji, 2008, 2009), or discrete element (Cook et al., 2004; Gil, 2005; Gil and Roegiers, 2006) approaches. They can be divided into two major groups: models that require a predefined direction for the hydraulic fracture process and models that can predict the fracture direction. Based on this classification, the following sections provide a description of the existing numerical models of hydraulic fracturing.

2.1 Models with Prescribed Fracture Direction

2.1.1 Continuum Approaches

Conventional hydraulic fracture models were developed to design hydraulic fracturing treatments

in the 1960s. In these models, fracture was simulated based on the material (volume) balance of the injected fluid (Howard and Fast, 1970). The fracture volume at each time was equal to the total volume of the injected fluid minus the volume of the fluid that leaked from the fracture walls into the reservoir. The assumed fracture shape and pressure distribution in the fracture can be used to calculate the fracture length and width (Howard and Fast, 1970; Gidley et al., 1989; Ji, 2008). The most popular two-dimensional fracture models are the Carter's, Perkins-Kern-Nordgren (PKN), and Geertsma-de Klerk-Khristianovich (GDK) (Howard and Fast, 1970) models, which mainly differ in their basic assumptions. Conventional hydraulic fracturing models do not consider all the complex features (e.g., poroelasticity, plastic deformation, and shearing around a fracture) involved in fracturing and may not be adequate for simulating hydraulic fracturing in unconsolidated oil sands (Settari, 1988; Ji et al., 2004; Xu et al., 2010).

In early hydraulic fracture models, fracture equations were solved independently of the reservoir equations by using an overall coefficient for the leak-off (Settari et al., 1990). Settari et al. (1990) proposed the partial coupling of the fracture and reservoir flow. The fracture equations were solved numerically during propagation. A fracture grid was created that was dynamically independent of the reservoir grid. The leak-off was calculated for each element using an analytical/numerical model. Then, the average transmissibility of the reservoir blocks containing the fracture were calculated and transferred to the reservoir model. The conventional reservoir model treated the fracture as a stationary fracture (Settari et al., 1990). Settari et al. (1992) showed that a dynamic fracture with multiphase flow can be simulated by the dynamic enhancement of the transmissibilities in the fracture plane.

A fracture model comprised of a geomechanical tool linked with a reservoir simulator can be an effective fracture modeling tool. In this model, the fracture is treated as a highly permeable portion of the reservoir (Settari et al., 2002a, 2002b), and the fracture conductivity is combined with the permeability or transmissibility of the reservoir grid containing the fracture.

Ji et al. (2009) simulated fracture propagation implicitly by applying pressure on the fracture face. Fracture face displacements caused by the fracturing pressure were used to calculate the permeability multipliers. Moreover, the reservoir and geomechanical/fracturing modules were coupled iteratively.

By assuming the fracture direction in an impermeable rock, Papanastasiou (1997a; 1997b; 1999) solved the continuity equation in conjunction with the lubrication theory (which relates the pressure gradient to the fracture width for a viscous Newtonian fluid) and ignored the leak-off from the fracture into the rock matrix. van Dam et al. (2000) used a similar approach to solve the Poiseulle law and continuity equation. In one of the most recent published works involving this approach, Wang et al. (2017) utilized a mesh-free SPH method in conjunction with a size-dependent continuum constitutive model to investigate the Mode-I fracture behavior of a rock

formation.

2.1.2 Continuum-Discontinuum Approaches

The continuum-discontinuum group of hydraulic fracture models includes special types of elements such as thin-layer solid elements or zero-thickness joint elements. To place these special types of elements within the model, it is necessary to know the fracture direction and location.

Xue et al. (2006) performed a coupled analysis of hydraulic fracturing using ABAQUS (based on the finite element method and cohesive elements using damage mechanics). Zhang et al. (2010) used ABAQUS to simulate a staged fracturing of a horizontal well in a thin pay zone. Their model included perforations, wellbore casing, cement, the pay zone, cap rocks, base rocks, a micro-annulus fracture, and a vertical transverse fracture. They found that the micro-annulus fracture and the transverse fracture occurred simultaneously in the early stages of the process. The micro-annulus was then closed owing to a higher stress concentration around the wellbore, whereas the transverse fracture propagated. It is worth noting that micro-annulus fractures resemble the multiple fractures observed in laboratory experiments and in the field .

Lian et al. (2006) simulated hydraulic fracturing using ABAQUS and found that permeability is more important in the fracture tip than in other locations. Their study indicated that the void ratio of the medium reached the maximum value (in the model) at the fracture tip, resulting in a permeability increase. Similar results have been reported by other researchers (Khodaverdian and McElfresh, 2000; Wu, 2006). This permeability enhancement may assist in the shearing process and increase the fracturing pressure.

2.2 Models without a Prescribed Fracture Direction

The hydraulic fracture models that do not need a predetermined fracture direction are divided into two major groups: discontinuum and continuum models. In the discontinuum group, the DEM is used to simulate the rigid grains or deformable blocks and the interface between them. These types of models are impractical in terms of their solution times and are incapable of simulating field-scale problems because of the large number of particles/blocks that they involve.

In the continuum models, the fracture is smeared and the equivalent properties of the fracture and matrix, such as the permeability and porosity, are assigned to the continuum mesh. This approach makes it possible to model fracture flow, matrix flow, and the stress/strain effect on permeability in a fully or partially coupled manner. This method has been used to simulate fracturing processes such as solid waste injection in soft rock reservoirs (Chin and Montgomery,

2004) and the fracturing of unconsolidated sands (Zhai and Sharma, 2005; Zhai, 2006; Xu, 2010).

2.2.1 Discontinuum Models (Discrete Element Models)

Cook et al. (2004) used a 2D DEM code, MIMES (Modeling Interacting Multibody Engineering Systems (Rege, 1996)), and extended it to fracture propagation during an experimental slurry injection in the Berea Sandstone (loosely cemented sandstone).

Cook et al. (2004) showed that similar to their experiments, multiple fractures can occur when the two principal stresses are equal, leading to a higher storage capacity of the fractured medium. In the case of different horizontal stresses, a distinct fracture occurs parallel to the direction of the maximum horizontal stress (Cook et al., 2004). Although this model can simulate the proper fracturing modes, it is limited because of its small size.

Gil (2005) and Gil and Roegiers (2006) developed a DEM model using PFC3D to determine the potential and importance of the shear failure mechanism and the effect of leak-off during hydraulic fracturing in poorly consolidated sandstones (Anter sandstone). Gil (2005) found that shear failure seems to be more important than tensile failure for these rocks.

At higher differential pressures (17 MPa), the effect of viscosity was marginal and the results of all of the models were similar (Gil, 2005; Gil and Roegiers, 2006). The results showed that for the Anter Sandstone (a weakly-consolidated sandstone near Ardmore, Oklahoma), shear failure is the dominant failure mechanism during hydraulic fracturing. This may explain why the field fracturing pressure is much larger than what is predicted for unconsolidated sands (Gil, 2005; Gil and Roegiers, 2006). Although this model is capable of capturing the discontinuous nature of the fractures, permeability/porosity changes, and failure modes, it can only be used for small-scale problems.

As a few examples of more recent simulations using discontinuum-based models, Duan et al. (2018) modeled hydraulic fracture in permeable rocks using a DEM method and investigated the effects of viscosity, the injection rate, and the in situ conditions. Nguyen et al. (2017) proposed a DEM method using a cohesive model to couple damage mechanics with plasticity theory to analyze the fracturing behavior of soft rocks.

2.2.2 Continuum Models

2.2.2.1 Discrete Fracture Approach

The discrete fracture approach can be used to simulate induced fractures. In this approach, nodal grafting or the node-splitting technique (Pak, 1997) is implemented and an induced crack can pass through the boundaries of the elements or inside of the elements.

To permit fracture propagation at the element interfaces, a suitable shape function is added to the element interpolation functions. These additional shape functions can sometimes make the elements incompatible and produce mesh locking (Pak, 1997). This method works well in situations wherein the number of dominant fractures is limited. In this regard, Zhou et al. (2016) used a coupled DFN-DEM model for the simulation of hydraulic fracture and natural fracture interactions.

Pak (1997) and Pak and Chan (2004) developed a 2D finite element thermo-hydro-mechanical numerical model (continuum discrete fracture model) of hydraulic fracturing in oil sands and used the model to simulate large-scale hydraulic fracturing experiments. In a finite element model using the node-splitting technique, double nodes with the same coordinates were placed in areas prone to cracking. When tensile or shear failure occurred, the double nodes split into two separate nodes. This method can be used to propagate a fracture through the model. Pak (1997) used fracture elements to simulate fluid or heat flow inside of a fracture such that when four of six nodes of the fracture element were split, the fracture scheme was activated and a finite value for the permeability was assigned to the element. The results showed that a fracture can be initiated by tension. Additionally, it was shown that in the case of a highly porous reservoir with high permeability, a single planar fracture is unlikely to occur, and the fracture pattern will appear in the form of a fractured zone with a network of interconnected and tiny fractures (Pak and Chan, 2004).

This model provides a basis for understanding the overall behavior of hydraulic fracturing in unconsolidated sand, but it does not accurately capture the mechanical behaviors (such as frictional sliding or opening) of shear/tensile fractures. Additionally, in this model, the permeability of a tensile fracture is not dependent on its width.

2.2.2.2 Smeared Fracture Approach

In the smeared fracture approach, the medium, including the fractured and intact rocks, is treated as a continuum, and the actual stresses and strains are averaged over a certain representative volume known as the crack band. In this approach, the fracture is simulated by altering the physical and mechanical properties of the elements that satisfy the fracturing criteria. The smeared crack model is expressed as a cracked material with equivalent anisotropic continuum properties that are degraded in the crack band (Klerck, 2000).

Researchers have proposed different methods to model a smeared crack fracture in concrete. The

fixed crack (Bažant and Oh, 1983), orthogonal fixed crack (Klerck, 2000), rotating crack (de Borst and Nauta, 1985), and stabilized rotating crack (Bažant, 1984; de Borst and Nauta, 1985) models have been proposed to consider single or multiple cracks in smeared crack modeling. A detailed review of these models can be found in Klerck (2000). The fixed crack model is overly stiff with induced shear stresses (shear response) and is unable to account for the effective crack reorientation because the orientation of the crack band and the axes of orthotropy (i.e., of material behavior) are fixed at the onset of softening (Klerck, 2000).

Roostaei et al. (2019) developed a coupled hydro-mechanical model using a smeared fracture model and an in-house reservoir simulator. They reported on their model's ability to capture both tensile and shear fractures in a formation.

The smeared fracture approach enables simulation of the discrete nature of fractures, which is accomplished by reducing the stiffness of the fractured elements, especially in tensile fractures. However, this approach requires modifying the permeability and porosity of the fractured elements. Therefore, finding suitable formulas for the shear or tensile fracture permeability is of paramount importance. As will be shown later, the main difference between smeared hydraulic fracture models is the approach using which the shear/tensile-related permeability enhancement is calculated. Fracture permeability can be a function of effective stress, pore pressure, strain, porosity, and saturation. In some of the existing hydraulic fracture models, the equivalent permeability of a fractured element is a function of the effective stress or pore pressure, whereas in others, it is calculated as a function of the displacement of the fractured elements.

Using Drucker-Prager plasticity, Chin and Montgomery (2004) developed a 3D finite element model to simulate solid waste injection in unconsolidated sandstone reservoirs using the smeared fracture approach. They assumed that when the pore pressure was larger than the minimum stress in any element, local confined fracturing would occur.

Zhai and Sharma (2005) and Zhai (2006) developed an iteratively coupled 2D finite difference model for fracturing in unconsolidated sand. The porosity and permeability were empirical functions of the volumetric strain and effective stress

Zhai and Sharma (2005) and Zhai (2006) concluded that in a normal faulting regime in unconsolidated sand, shear failure is either the dominant or, more likely, the sole fracturing mechanism. Tensile failure/fracture may occur at injection pressures that exceed the vertical stress (i.e., the maximum principal stress). In the strike-slip regime, shear failure was also concluded to be the dominant mechanism with tensile failure/fracture only occurring in the near-wellbore region due to higher pore pressures (Zhai and Sharma, 2005).

Xu et al. (2010) performed a 3D fully coupled finite element simulation (smeared approach) of field-scale hydraulic fracturing in unconsolidated oil sands. In their model, the smeared fracture

approach was used in which permeability was a function of porosity (Kozeny-Carman equation) as well as saturation (relative permeability). Xu (2010) and Xu and Wong (2010) showed that a high permeability zone (in which the predominant mode of failure is shearing), resulting from fracturing, propagates out from an injection well similar to a tensile hydraulic fracture. This model, however, does not adequately differentiate between the fluid flow behavior of shear and tensile fractures. In this model, the equivalent plastic strain (and not the plastic tensile strain) controls the permeability changes due to fracturing. This model functions well if shear failure occurs in a diffused form and if it is the main mechanism of fracturing.

2.3 Assessment of the Existing Tools and Approaches

The major mechanisms and processes involved in the hydraulic fracturing of the previously mentioned weak and unconsolidated sandstones must be considered in a numerical hydraulic fracturing model. Most of the current continuum-based numerical models for simulating hydraulic fracturing in weak or unconsolidated sandstones require a predetermined hydraulic fracture direction (Papanastasiou, 1997b; Lian et al., 2006; Xue et al., 2006; Ji et al., 2009; Zhang et al., 2010). Although some recent continuum models have been adapted to capture fractures in general directions (Pak, 1997; Zhai, 2006; Xu, 2010), they lack a proper tensile fracture-flow law or do not simulate the development of shear bands and their interactions with the tensile fractures (Pak, 1997; Zhai, 2006; Xu and Wong, 2010).

Within the framework of continuum mechanics, the discrete fracture and the smeared fracture methods are the two approaches that have been extensively used to simulate hydraulic fractures. In the discrete fracture modes, interface/cohesive elements are used to simulate the fractures. Some restrictions, however, are of concern in these models: (1) the logic of these programs may break down if large numbers of interfaces are included in the simulation; (2) new contacts cannot be detected automatically; and (3) the models are based on small displacements and/or rotations (Nagel et al., 2011).

In determining whether a discrete or smeared fracture approach should be used, the computational effectiveness of each method must be considered (Bažant and Oh, 1983). The discrete approach involves some computational disadvantages. For instance, fracturing increases the number of nodes and changes the topological connectivity of the mesh, which creates significant challenges for automating such an approach (Suidan and Schnobrich, 1973; Bažant and Oh, 1983). Even though the smeared fracture approach does not fully represent the physical nature of a crack, it is an alternative to the discrete fracture method because it enables the simulation of fracture branching, fracture rotation, and multiple shear and tensile fractures in un-predetermined directions.

In the hydraulic fracturing of unconsolidated sand such as in the oil sand reservoirs in Alberta, a single fracture is unlikely to occur, and the result of fracturing is a high porosity zone consisting of a network of micro-cracks (Pak, 1997; Xu et al., 2010). Continuum mechanics is suitable for modeling hydraulic fracturing in such formations (Xu et al., 2010). Fracturing in weak or unconsolidated sandstones occurs in the form of a zonal fracture rather than a planar fracture (Pak, 1997; Xu et al., 2010). A suitable simulation must account for the strong non-linearity that arises from shear-induced dilation, tensile parting, and variation of the fluid mobility (Xu et al., 2010).

3 Model Formulation

3.1 Material Constitutive Model

A bilinear Mohr–Coulomb shear model with strain hardening/softening is employed in this study to address the shear strength of the material. The yield surfaces can be described using the following equation (Nouri et al., 2009; Jafarpour et al., 2012):

$$F = T - (q + P)\mu = 0 \,, \tag{1}$$

where P is the mean effective stress and T is the square root of the second invariant of the deviatoric stress tensor in an axisymmetric state of stress (as in a triaxial compression experiment). P and T are defined as

$$P = (\sigma_z' + 2\sigma_r')/3 \,, \tag{2}$$

$$T = |\sigma_z' - \sigma_r'|/\sqrt{3} \,, \tag{3}$$

where σ_z' and σ_r' are effective axial and radial stresses, respectively and μ is the friction coefficient, which is equal to $\tan\phi_\sigma$. This parameter is related to the friction angle (ϕ_a) via the following equation:

$$\tan\phi_\sigma = \frac{2\sqrt{3}\sin\phi_a}{3 - \sin\phi_a} \tag{4}$$

This model has been calibrated against triaxial experiments. Further description of the model parameters and the detailed calibration process can be found in Taghipoor et al., 2014. A cohesive constitutive model (Barenblatt, 1962) is used to calculate the tensile strength of the material. It is assumed that before fracturing, the rock undergoes linear softening under tension

(Fig. 1).

An element is subjected to tensile fracturing if the following requirements are met at the same time:

(i) The element's tensile strength is degraded altogether and the element is exposed to the tensile stresses.

(ii) Other fractured elements link the element to the injection source (connectivity condition).

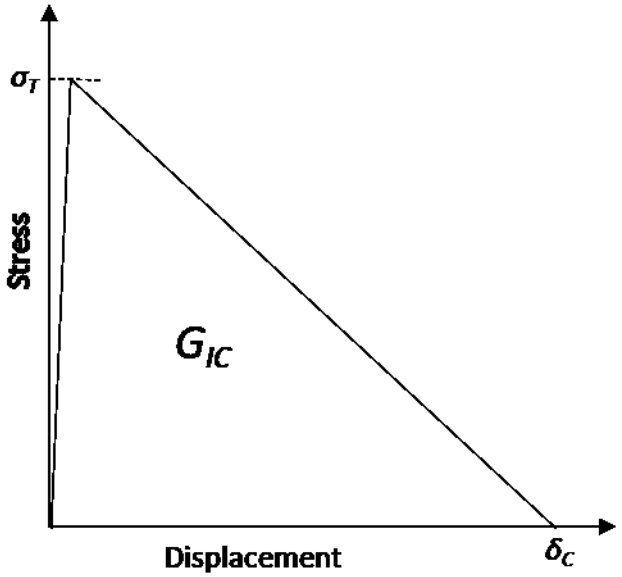

Fig. 1. Cohesive behavior of a fracture (Papanastasiou, 1999).

3.2 Smeared Tensile Fracture-Flow Model

For fluid flow in a smeared tensile fracture, a slightly modified version of the procedure proposed by Ji (2008) and Ji et al. (2009) is used by implementing the tensile strain of the fractured element instead of the fracture aperture, as shown below.

$$\mathrm{PM} = 1 + \frac{1}{12 F_{\mathrm{rough}} K_{\mathrm{m}}} \varepsilon_{\mathrm{T}}^{3} t^{2} \tag{5}$$

Here, ε_{T} is the tensile strain in the element, t is the equivalent element thickness in the direction of the tensile strain, F_{rough} is the fracture wall roughness, and K_{m} is the matrix permeability.

The permeability multiplier, PM, is determined using the cubic law for the smeared fracture when a tensile fracture is detected in an element at any time step in the solution. This multiplier is then applied to the permeability in the direction of the fracture orientation, whereas the

permeability in the direction normal to the fracture remains the same or follows the shear permeability criteria if shear failure is present. The resulting orthotropic permeability tensor is rotated back to the global coordinate system, which forms an anisotropic permeability tensor for the fractured element.

3.3 Smeared Shear Failure Flow Model

Touhidi-Baghini's model is described by Eq. (6) with different B values in the horizontal and vertical directions. It is employed to address the alterations in permeability induced by shear dilation in the hydraulic fracture model.

$$\ln\frac{k}{k_0}=\frac{B}{\phi_0}\varepsilon_{\mathrm{v}} \tag{6}$$

Here, k and k_0 are the current and initial permeabilities of the material, respectively; ε_{v} is the volumetric strain; B is the rate at which the permeability evolves as a function of the volumetric strain variance; and ϕ_0 is the initial value of porosity.

Touhidi-Baghini's model has been validated against permeability measurements in triaxial compression tests of a weakly consolidated sandstone in the elastic compression range. This calibration can be found in Appendix A.

The width of the tensile fracture is a solution-dependent parameter and is calculated and updated at each time step based on nodal displacements. Fracture energy regularization (Taghipoor et al., 2015) has also been implemented to reduce the impact of the mesh size.

3.4 Fluid Flow Model

Darcy's law for fluid flow in porous media is used to solve for the flow in the intact matrix, tensile fractures, and shear failure:

$$q_i=-\frac{K_{ij}}{\mu}\frac{\partial}{\partial x_j}(p-\rho_{\mathrm{f}}g_k x_k) \tag{7}$$

Here, $\boldsymbol{q}$ is the specific discharge vector, x is the coordinate, K_{ij} is the permeability, μ is the fluid viscosity, p is the fluid pressure, ρ_{f} is the mass density of the fluid, the subscript k = 1, 2 are the two components of the gravity acceleration vector, and the subscripts i and j = 1, 2 are indices used for two-dimensional analysis.

Flow analysis is conducted by constructing a flow model using a point-distributed grid. The solution can be obtained by applying the initial reservoir pressure, assigning no flow to the

symmetry boundary, assigning a prescribed injection flow rate at the wellbore, and designating a pressure boundary for the remaining reservoir boundaries.

3.5 Porosity Change

Changes in porosity are related to the volumetric strain, which can be calculated using the following geomechanical model (Touhidi-Baghini, 1998):

$$\phi = \frac{\varepsilon_v + \phi_0}{1 + \varepsilon_v}, \tag{8}$$

where ϕ and ϕ_0 are the initial and current porosities, respectively, and ε_v is the volumetric strain. An element is considered to experience tensile fracture if the tensile strength of the element has degraded completely. The permeability of an element that undergoes tensile fracturing is calculated using the permeability multiplier.

3.6 Improving the Numerical Stability

According to the cubic law, fracture permeability is a third-degree function of the fracture aperture. Numerical instability is expected in the case of a sudden increase in permeability, extending from the matrix to the permeability of the fracture. Therefore, numerical stability must be improved by increasing the fracture permeability at each iteration until a converged solution is achieved, as proposed by Ji (2008). This approach is also used in this study to address this problem, and both the fracture and matrix permeabilities are determined using this approach.

In the scheme proposed by Ji (2008), the non-modified permeabilities of a tensile fracture and shear failure are calculated for the current iteration, denoted as *v*. If the solution does not satisfy the convergence criteria, the permeabilities are updated in the next iteration, *v*+1, using Eq. (9). The iterative process continues, and the calculations are repeated until the maximum errors are below an error margin of 2% for all of the variables at the same time.

$$k_i^{v+1} = \alpha k_i + (1 - \alpha) k_i^v \tag{9}$$

Here, α is a damping factor, k is the principal permeability in direction i, and v is the previous iteration number. A smaller damping factor enhances the numerical stability of this process; however, the model run time will be correspondingly extended.

3.7 Examination of mesh dependency

The post-failure responses of weakly consolidated sandstone at low effective confining stresses exhibit severe strain softening and localization (softening refers to a decrease in the material's load-bearing capacity). The shear strain-softening behavior of a rock-type material at a low effective confining stress (LECS) (Sulem et al., 1999; Bésuelle et al., 2000) and the localization in tension (Klerck, 2000) have been investigated extensively in literature. These behaviors are expected to be the predominant modes of failure/fracture around injection points in hydraulic fracturing processes in weakly consolidated sandstones. Degradation in the tensile/shear band in weakly consolidated sandstones is localized within a width that is equal to the characteristic length of the material and is a function of the grain size (Crook et al., 2003).

A regularization technique, which is referred to as fracture energy regularization, is employed because the Mohr–Coulomb plasticity model with/without softening does not consider the effects of the element sizes. In this approach, energy that is dissipated as the fracture surfaces are formed is ensured to be mesh invariant, and the effects of size are taken into consideration in this formulation (Crook et al., 2003). This technique appears to be simple and easy to implement, and it can be employed in the regularization of the energy dissipated in both Mode-I and model II fractures (Cook et al., 2004).

To attain mesh independency of the localization in this model, the approach described by Crook et al. (2003) is implemented. The approach builds on the work performed by Bažant and Oh (1983), Pietruszczak and Mróz (1981) (for Mode II fractures), and Klerck (2000) (for Mode-I fractures). It is based on the concept that the fracture energy release rate, which is defined as the energy dissipated in the formation of new fracture surfaces, is invariant within various numerical mesh sizes, as illustrated in Fig. 2.

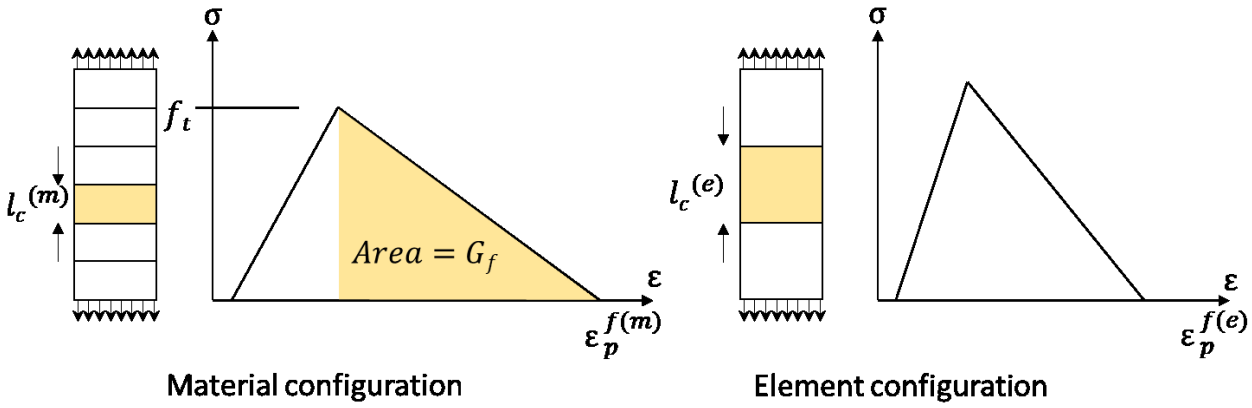

Fig. 2. Fracture energy dissipation (Crook et al., 2003).

The following two hypotheses form the basis of the fracture energy method (Nouri et al., 2009):

(i) Bažant and Oh (1983) found that in a strain-softening material, a sharp inter-element crack and a smeared crack provide essentially the same energy release rate.

(ii) In standard strain-softening modeling techniques, deformations are concentrated in narrow bands that collapse down to the smallest width that can be resolved by the mesh. If the element size is selected to be equal to the bandwidth, the fracture energy can be estimated accurately.

The fracture energy is kept constant through modifications of the plastic shearing strain intensity for the elements with sizes that are larger than the shear bandwidth using the following equation:

$$g^{\mathrm{p(e)}} = g^{\mathrm{p(m)}}[\frac{l_{\mathrm{c}}^{(\mathrm{m})}}{l_{\mathrm{c}}^{(\mathrm{e})}}]^{n} \tag{10}$$

Here, $l_{\mathrm{c}}^{(\mathrm{m})}$ is the material characteristic length equivalent to the shear band thickness, $l_{\mathrm{c}}^{(\mathrm{e})}$ is the element characteristic length defined as the diameter of the circle (sphere) with an area (volume in 3D) equal to that of the element being considered, and g^{e} and g^{m} are the inelastic fracturing strains (plastic shear strain for Mode II fractures and plastic tensile strain for Mode-I fractures) of the material and element, respectively; n is a material constant and is equal to 1 when LEFM are assumed. This assumption seems to be valid for Mode-I fractured rock and concrete (Crook et al., 2003). As the fracture length changes, some rock types exhibit a varying energy release rate (Bažant et al., 1993), which may be addressed by using an R-curve that represents the material resistance to the crack propagation (Anderson, 1991). The responses of these materials are not consistent with the LEFM assumption, which requires the parameter n to deviate from the value of 1.

Crook et al. (2003) emphasized that this localization limiter is only valid when $l_{\mathrm{c}}^{(\mathrm{e})} \geq l_{\mathrm{c}}^{(\mathrm{m})}$, indicating that the width of the localization band must be less than or equal to the element characteristic length, which is usually the case in the simulation of field fracturing processes.

Equivalent plastic strain (EPS), which is also referred to as plastic shear strain, is formulated using the following equation (Itasca Consulting Group Inc., 2011):

$$g^{\mathrm{p}} = \frac{1}{\sqrt{2}}[(\Delta e_1^{\mathrm{ps}} - \Delta e_{\mathrm{m}}^{\mathrm{ps}})^2 + (\Delta e_{\mathrm{m}}^{\mathrm{ps}})^2 + (\Delta e_3^{\mathrm{ps}} - \Delta e_{\mathrm{m}}^{\mathrm{ps}})^2]^{1/2} \tag{11}$$

where $\Delta e_{\mathrm{m}}^{\mathrm{ps}}$ is the volumetric plastic shear strain increment, which is defined as

$$\Delta e_{\mathrm{m}}^{\mathrm{ps}} = \frac{1}{3}(\Delta e_1^{\mathrm{ps}} + \Delta e_3^{\mathrm{ps}}) \tag{12}$$

and Δe_j^{ps}, (j=1, 2 and 3) are the principal plastic shear strain increments. Here, Δe_2^{ps} is equal to zero for the plastic strain assumption. For tensile-softening behaviors, EPS will be equal to the

plastic tensile strain increment, Δe_3^{pt}.

Implementing this method in a numerical model does not require any modification of the standard numerical technique. To implement Eq. (10), a good estimation of the material characteristic length, $l_{\mathrm{c}}^{(\mathrm{m})}$, or the shear/tensile band thickness is required. Experiments have shown that the thicknesses of both the tensile and shear bands can be on the order of the grain size of the examined material. Sulem et al. (1999) suggested a shear band thickness of 10 to 16 times the average grain size. Based on previous studies, Desai (2001) concluded that for a geological material, the width of a shear band is around 10 to 30 times the average grain diameter. Based on experimental observations, Wolf et al. (2003) suggested that the band thickness may be up to 6 to 13 times the average grain size in granular materials. Bažant and Oh (1983) proposed a tensile band thickness three times the sizes of the aggregates in concrete. If the average grain size of the weakly consolidated sandstone is known, it is possible to estimate an approximate material characteristic length.

4 Verification of the Model

In this section, the proposed smeared fracture approach is implemented and utilized in a numerical model based on the continuum mechanics assumption. This section presents the verification of the model using the numerical data reported by Papanastasiou (1997b), which is concerned with the simulation of hydraulic fracturing in an impermeable rock. Further validation and verification of the presented numerical model were reported by Taghipoor et al. (2014, 2015) and Roostaei et al. (2019).

4.1 Numerical Model Description

The smeared fracture methodology was implemented in FLAC (Itasca Consulting Group Inc., 2011). The flow and mechanical calculations were performed in FLAC using a sequentially coupled scheme. The hydraulic fracture was simulated in a plane-strain configuration, consistent with the work of Papanastasiou (1997b).

4.1.1 Material Properties

In his paper, Papanastasiou (1997b) considered three scenarios for an impermeable matrix: elastic with a static modulus, elastic with a dynamic modulus, and elastoplastic with cohesion hardening. The results of the verification of these three cases are presented here.

The rock was assumed to undergo linear softening under tension before fracturing, which is a cohesive behavior (Barenblatt, 1962), as shown in Fig. 1. This was consistent with the model that

Papanastasiou (1997b; Papanastasiou, 1999) used for the interface elements lying in the direction of the crack growth. Fracture energy regularization was applied to this tensile model to reduce the mesh dependency. A tensile strength of 0.5 MPa and a fracture toughness of 1.0 MPa $\sqrt{m}$ were considered for the material (Papanastasiou, 1997b).

The static and dynamic elastic moduli (E_{stat} and E_{dyn}) and the Poisson's ratio were equal to 1.785 GPa, 16.200 GPa, and 0.3, respectively. A friction angle of 28 degrees was considered, which was equal to the dilation angle for the associated behavior. The initial uniaxial compressive strength was 4 MPa, and a strain-hardening behavior was considered in which the equivalent stress (uniaxial compressive strength), σ_{e}, would increase with the accumulated plastic shear strain (Papanastasiou, 1997b). This was defined by:

$$\sigma_{\mathrm{e}} = \sigma_{\mathrm{e}}^{0} + h\varepsilon^{\mathrm{p}}, \tag{13}$$

where h is the linear hardening modulus, which is defined as

$$h = \frac{E_{\mathrm{stat}}}{1 - E_{\mathrm{stat}}/E_{\mathrm{dyn}}} \tag{14}$$

The viscosity of the injecting fluid was 100 cp. A very small permeability (10^{-15} md) was assigned to the matrix.

4.1.2 Model and Grid Size

The model height and width are 64 and 32 m, respectively. Only one wing of the fracture was simulated in the model, as shown in Fig. 3. The model does require the inclusion of an initial fracture, which was necessary in Papanastasiou's discrete fracture model. A uniform grid size of 20 m × 20 cm was used for the entire model except in an area of 4 m by 0.8 m around the injection point, as illustrated in Fig. 3. Three different grid sizes of 20, 10, and 5 cm were used in this area to evaluate whether the results were mesh-dependent.

4.1.3 Initial and Boundary Conditions

All model boundaries were fixed with respect to displacement in the normal direction. The maximum, intermediate, and minimum in situ stresses of 14, 9, and 3.7 MPa, respectively, were initialized in the model, as shown in Fig. 3. Following the initialization of the stresses, the fluid injection was applied at a constant rate of 0.0005 m^3/s. Every grid point was checked for tensile fractures at each time step. The permeability multiplier was calculated for the failed elements using Eq. (5).

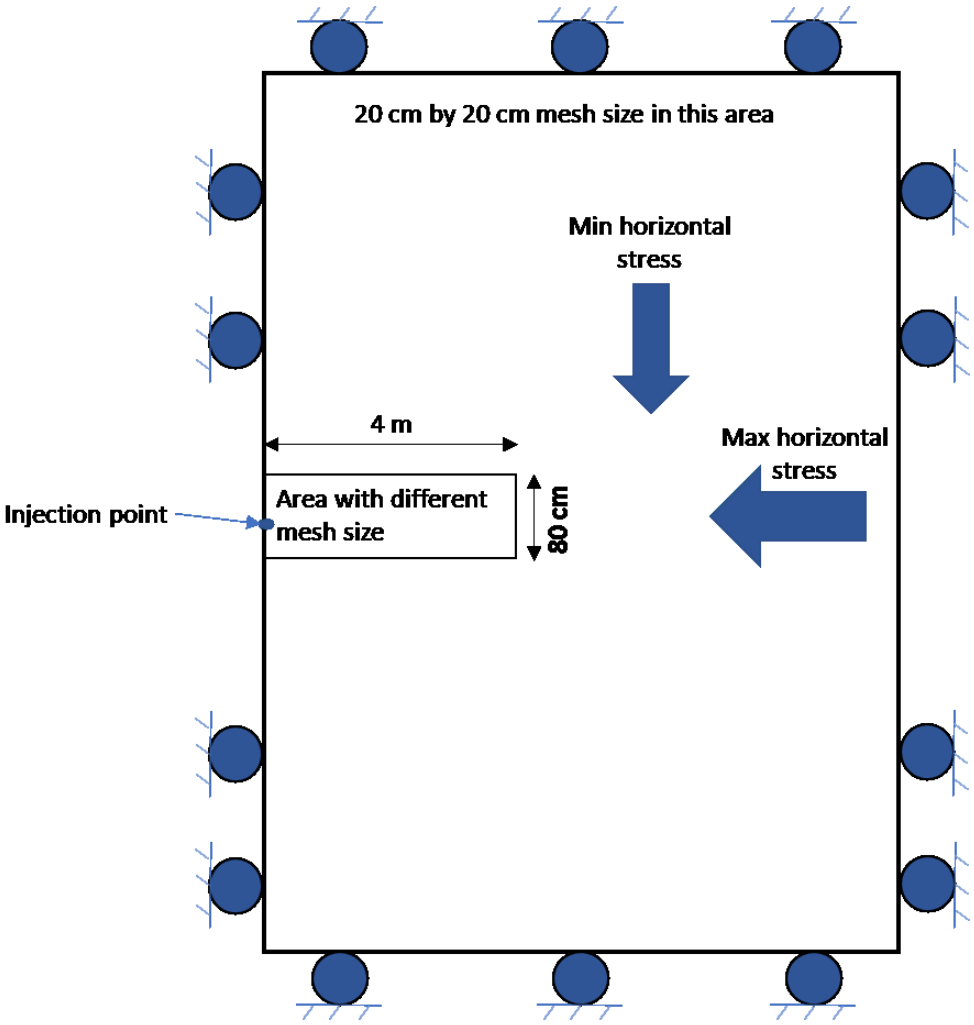

Fig. 3. Finite difference grid and boundary conditions.

The stress/strain solution is achieved when the unbalanced-to-applied force ratio for all of the grid points in the model becomes smaller than 0.001. The same tolerance was considered for the unbalanced fluid volume in the fluid flow analysis.

4.1.4 Numerical Modeling Results

Three different cases were considered for the purposes of verification, as determined by Papanastasiou (1997b): an elastic model with a static modulus, an elastic model with a dynamic modulus, and an elastoplastic model. Each case was analyzed using the three mesh sizes discussed in a previous section.

The fracture aperture in the developed smeared hydraulic fracture model is defined as the differential displacement of the two nodes containing a tensile fracture. Figure 4 compares the fracture aperture profiles for a fracture length of 2.40 m for both models. The elastic model with

a static modulus demonstrated a larger aperture along the entire fracture length. However, the model with a dynamic modulus resulted in a narrower fracture along a portion of the fracture. There is a reasonable agreement between the results of the proposed model and those of the Papanastasiou model (1997b).

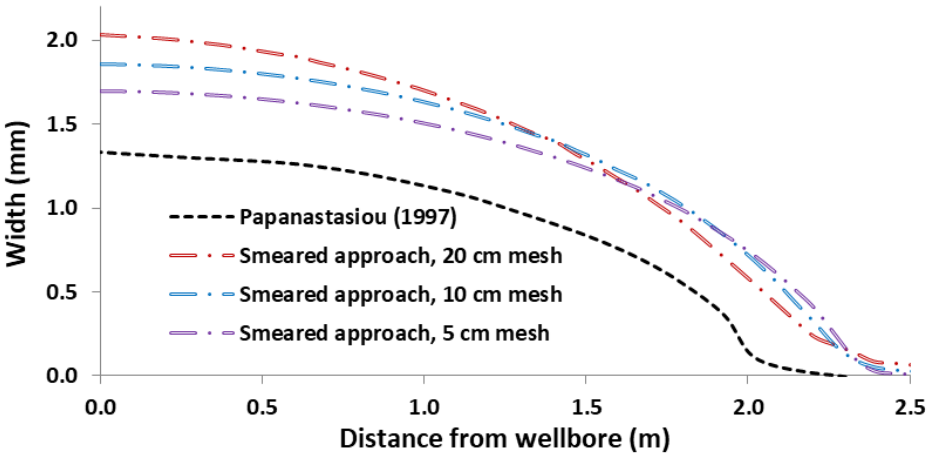

(a) elastic model with static modulus

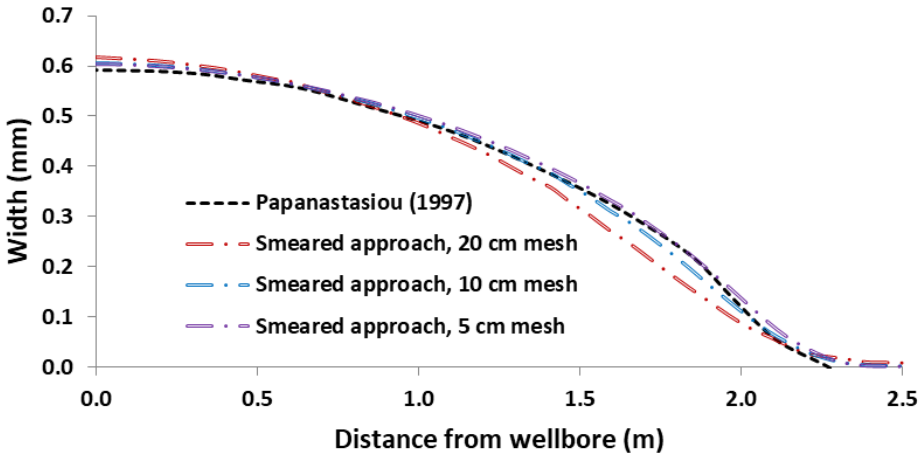

(b) elastic model with dynamic modulus

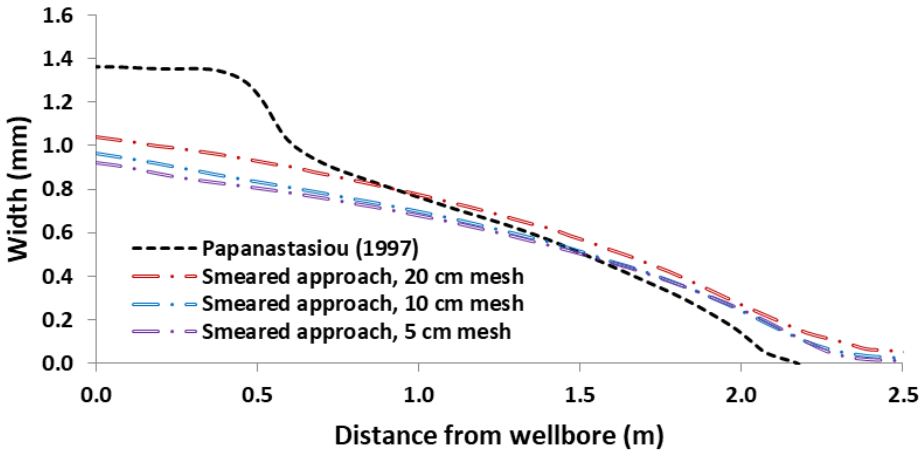

(c) elastoplastic model

Fig. 4. Fracture aperture for the three verification cases.

The elastoplastic model in Papanastasiou's work has a wider aperture near the injection point and a sharp decrease in the aperture at 0.5 m from the injection point, followed by a mild change in the aperture toward the fracture tip. The wide aperture that is close to the injection point may be due to the initial 0.5-m fracture used by Papanastasiou (1997b). An initial fracture of 0.5-m in length (without applying fluid pressure) prevents shearing and strain-hardening behavior in this area. This behavior is expected to occur when the fracture propagates from zero to 0.5 m. The initial fracture length influences the fracture aperture profile near the injection point, whereas the aperture profile is correctly calculated in the propagation interval (Papanastasiou, 1997b). Papanastasiou (1997b) emphasizes that any comparison of the fracture profile should be performed only within the propagation interval. Note that an initial fracture was not used in the smeared hydraulic fracture model proposed in this research.

Despite using fracture energy regularization to resolve the mesh dependency, some degree of the mesh-size effect was still observed in the results. This may partially result from the finite difference scheme used in FLAC (e.g., the pore pressures are averaged at the center of the finite difference elements). Weill and Latil (1992) reported similar mesh dependencies due to the smearing of the fracture permeability over the coarse elements. Even though the results showed some mesh dependency, reducing the mesh size demonstrated a converging trend in the computational results. This convergence was more significant in the cases of the elastic model with a dynamic modulus and in the elastoplastic model.

The net-pressure profiles inside of the fracture are plotted in Fig. 5, wherein the fracture has propagated to 2.40 m. The net pressure is defined as the fluid pressure inside of the fracture minus the minimum in situ stress. The very narrow fracture aperture near the fracture tip induces a high-pressure drop in this area, which is more significant in the case of the elastic model with a

dynamic modulus. The mesh dependency is still observed in the net-pressure profiles at the full propagation length. However, there is a good agreement between the results of the smeared fracture approach and the results of Papanastasiou's model (1997b). The smeared approach results tend to approach the results of Papanastasiou's model (1997b) when the mesh size is reduced.

For the three cases, the net pressure of the fracture at the injection point versus the fracture length is plotted in Fig. 6. The initiation-net pressures in the case of the elastic models with both static and dynamic moduli are in the range of 2.45 to 3.70 MPa for all three mesh sizes, whereas this value for the elastoplastic model lies in the range of 4.7 to 6.20 MPa. It can be concluded that the initiation pressure is significantly affected by the plastic behavior. This figure also shows that the predictions of the elastic model with a dynamic modulus are closer to those of the elastoplastic model; however, their mechanisms differ (Papanastasiou, 1997b). According to Papanastasiou (1997b), the large net pressure in the elastoplastic model is due to the dissipated energy in the plastic zones. However, in the elastic model with a dynamic modulus, a high net pressure is the result of a narrow aperture and a large pressure drop in this region.

For further propagation, the injection pressure reaches a maximum pressure in the range of 4.32 to 5.49 MPa for the static modulus case, and 8.34 to 13.34 MPa for the dynamic modulus case. These values for the elastoplastic model are 10.5 to 21 MPa. This indicates that the elastic modulus and elastoplastic behavior are determining factors for calculating the breakdown pressure.

An inconsistency is observed in the graphs for the elastoplastic model, wherein the fracture is between 0.5 and 0.75 m in length. Papanastasiou (1997b) used a 0.5-m initial fracture, whereas in our model, an initial fracture was not required. The inconsistency in the elastoplastic model appears to originate from the existence of this initial fracture, which prevented plastic deformation and shear hardening at the initiating stage. Regardless, a reasonable agreement is observed in the results, especially for the small-sized mesh.

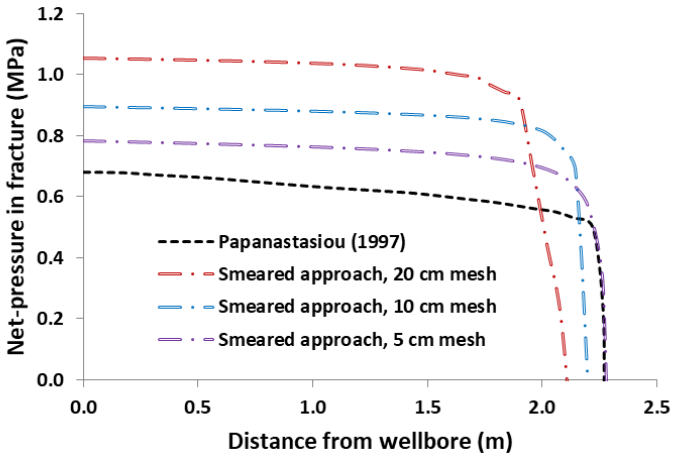

(a) elastic model with static modulus

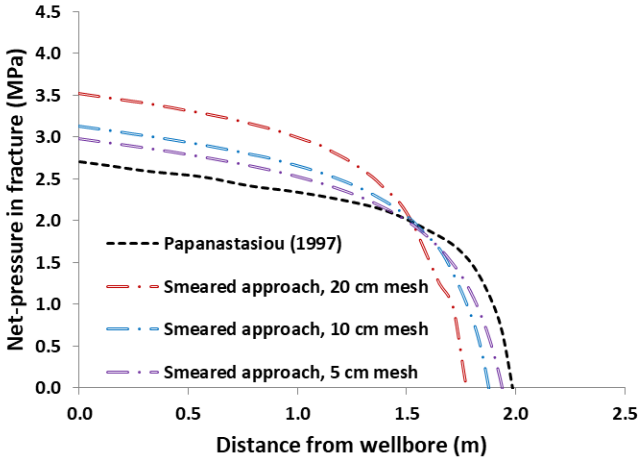

(b) elastic model with dynamic modulus

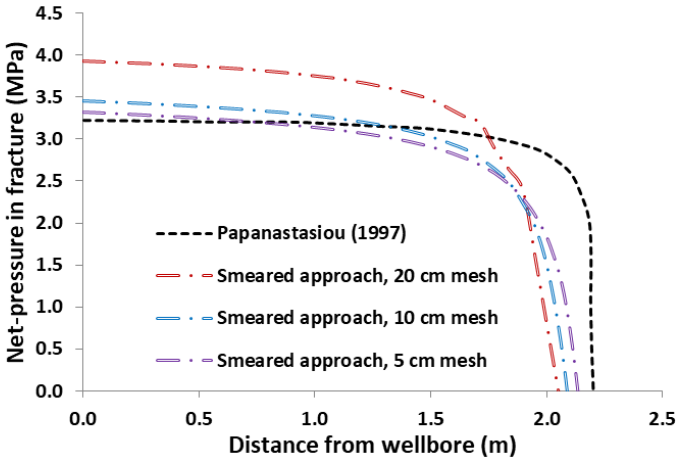

(c) elastoplastic model

Fig. 5. Fracture net-pressure profile for the three validation cases.

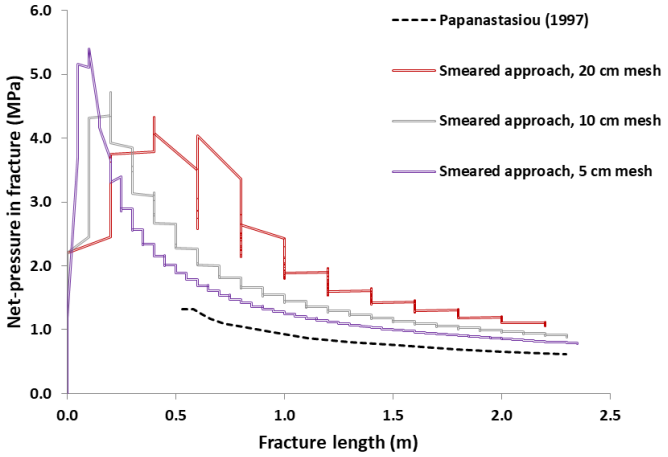

(a) elastic: static modulus

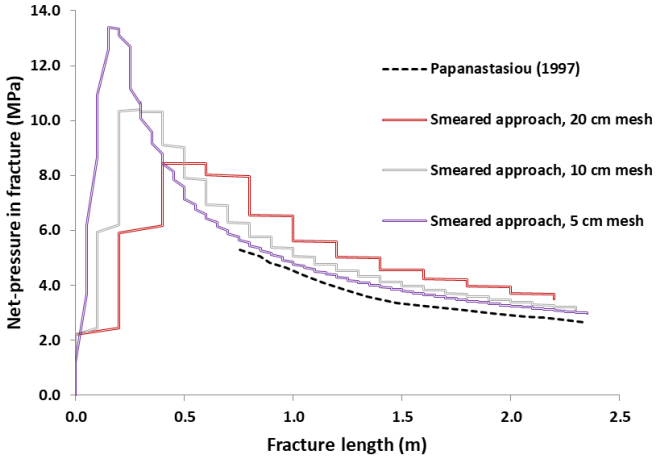

(b) elastic: dynamic modulus

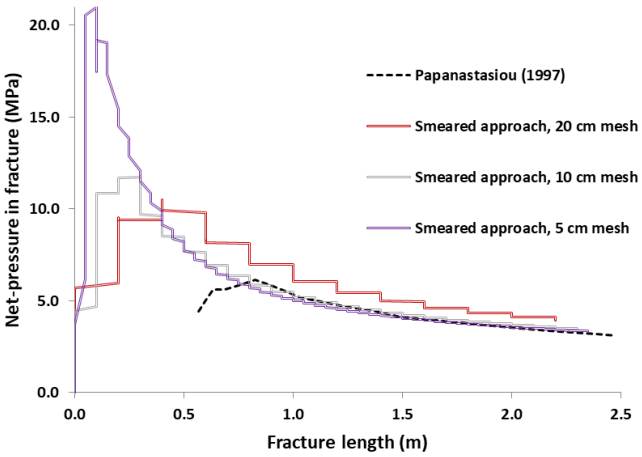

(c) elastoplastic

Fig. 6. Net pressure vs. the fracture length for the three verification cases.

To evaluate the effectiveness of the adopted regularization method, the results of the elastic model with a dynamic modulus, as well as those of the elastoplastic model, were compared with their un-regularized solutions. Although the regularization process had little influence on the fracture aperture compared to the corresponding un-regularized cases (Fig. 7), it affected the net fracturing pressure by about 0.5 MPa for all three mesh sizes, as shown in Fig. 8. It is clear that regularizing the fracturing energy is effective and produces results that are closer to those presented by Papanastasiou (1997b). The same trend is observed in both the elastic and elastoplastic models for all mesh sizes.

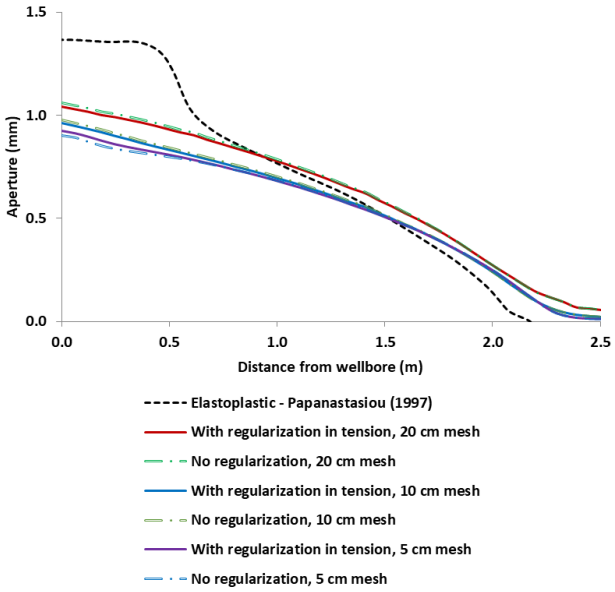

(a) elastoplastic

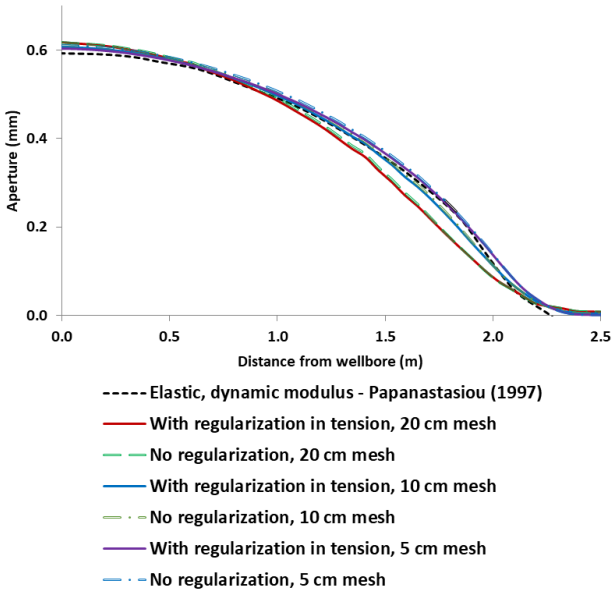

(b) elastic with dynamic modulus

Fig. 7. Comparison of the fracture apertures for the regularized and un-regularized static models with a dynamic modulus, as well as for the elastoplastic model.

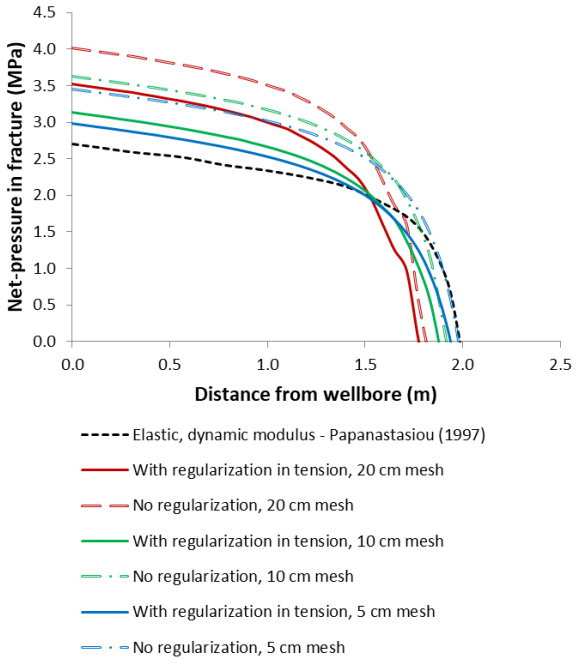

(a) dynamic modulus, examining regularization

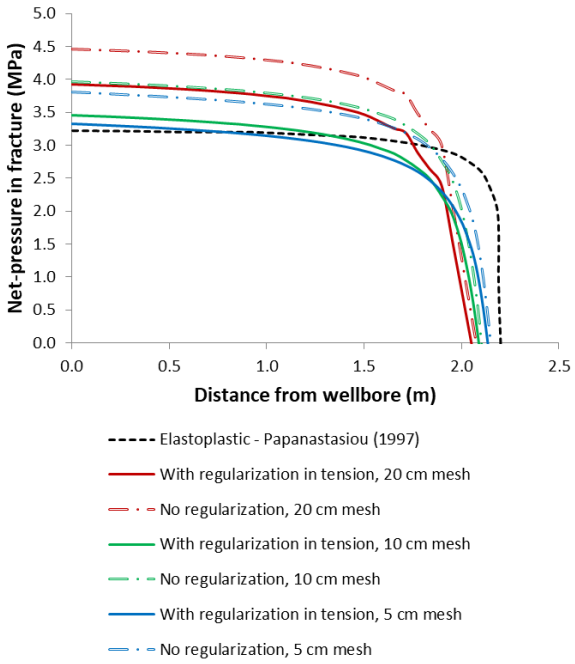

(b) elastoplastic, examining regularization

Fig. 8. Comparison of the net-pressure profiles for the regularized and un-regularized static models with a dynamic modulus, as well as for the elastoplastic model.

Figure 9 shows the ability of the model to determine the fracture pattern and yielded zones. The green, pink, and purple areas in the figure show previously yielded, at yield in shear, and at yield in tension elements in the model, respectively. The elements colored in purple indicate the induced hydraulic fracture.

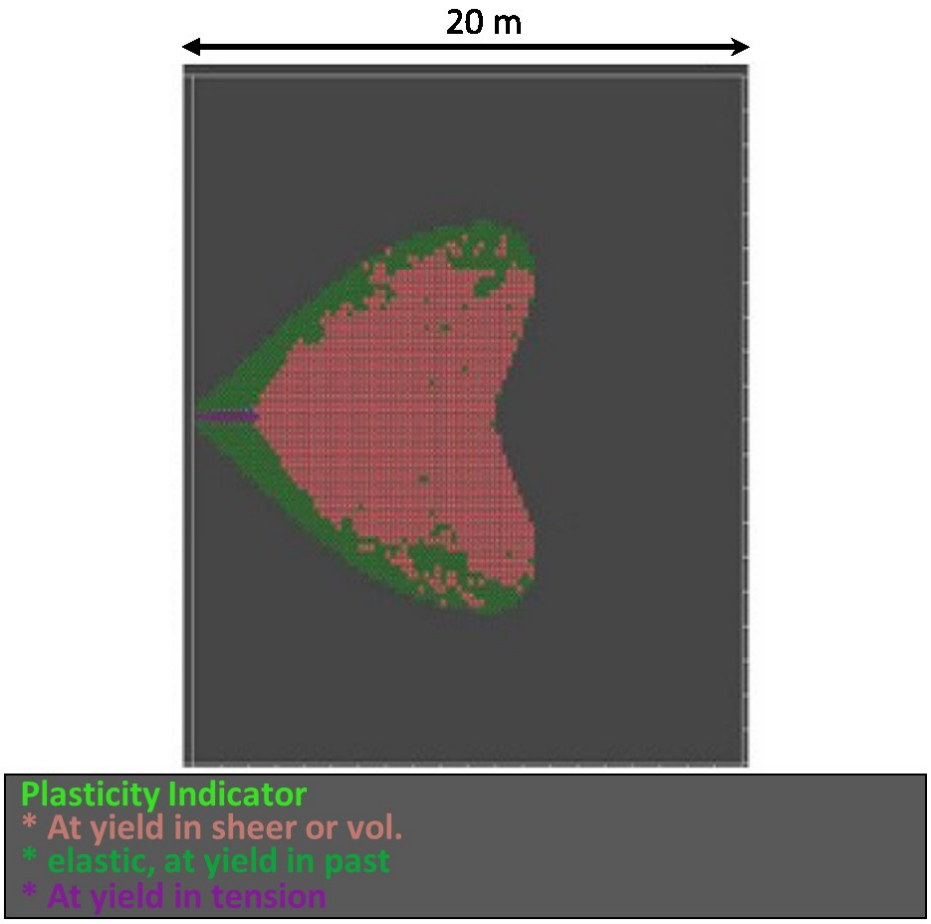

Fig. 9. Tensile and shear zones.

5. Field Application

Data from a series of well tests from the Burnt Lake project, located in the northeast Edmonton, were used to develop the numerical model in this study (Xu, 2010, Yeung and Adamson, 1991; Yeung, 1995). In this project, cyclic steam stimulation (CSS) was initially used as the proposed method of oil (crude bitumen) recovery from the Clearwater formation in the Cold Lake oil sands deposit. However, the project was suspended in the late 1980s as the price of heavy oil decreased at that time and the feasibility of other, lower-cost recovery options were investigated (Yeung and Adamson, 1991; Yeung, 1995).

A geological characterization of the project site was provided by Yeung (1995) and Xu (2010), which is described here. The target zone is in the Clearwater B sand with a pay thickness of 20 to 30 m. Well logs did not indicate the presence of a gas cap and no bottom water was detected except at the northeast corner of the lease property. The oil sands are unconsolidated and contain fine grains comprising 20% quartz, 20% feldspar, and 60% rock fragments, whereas 10%–20%

of the bulk volume comprises Smectite, Illite, Chlorite, and Kaolinite. A 4- to 5-m shale layer separates the overlying water-bearing layer in the Clearwater A sand from Clearwater B. Clearwater C is the underlying shaly layer of the reservoir, which is a very fine sand with interlayers of silt. A 3-m shale layer separates the Clearwater B and Clearwater C layers (Yeung, 1995). Three well tests were performed in the 178-mm diameter cased well 01-14-67-03W4 in the Burnt Lake project (Xu, 2010). The cased well was perforated at 5 m in the middle of the Clearwater B pay zone. Different injection rates were selected for the well tests, in which Test 3 has the highest applied pressure and Test 1 has the lowest. The bottom hole pressures (BHP) were recorded for all of the tests at different flowrates, which are illustrated in Fig. 10.

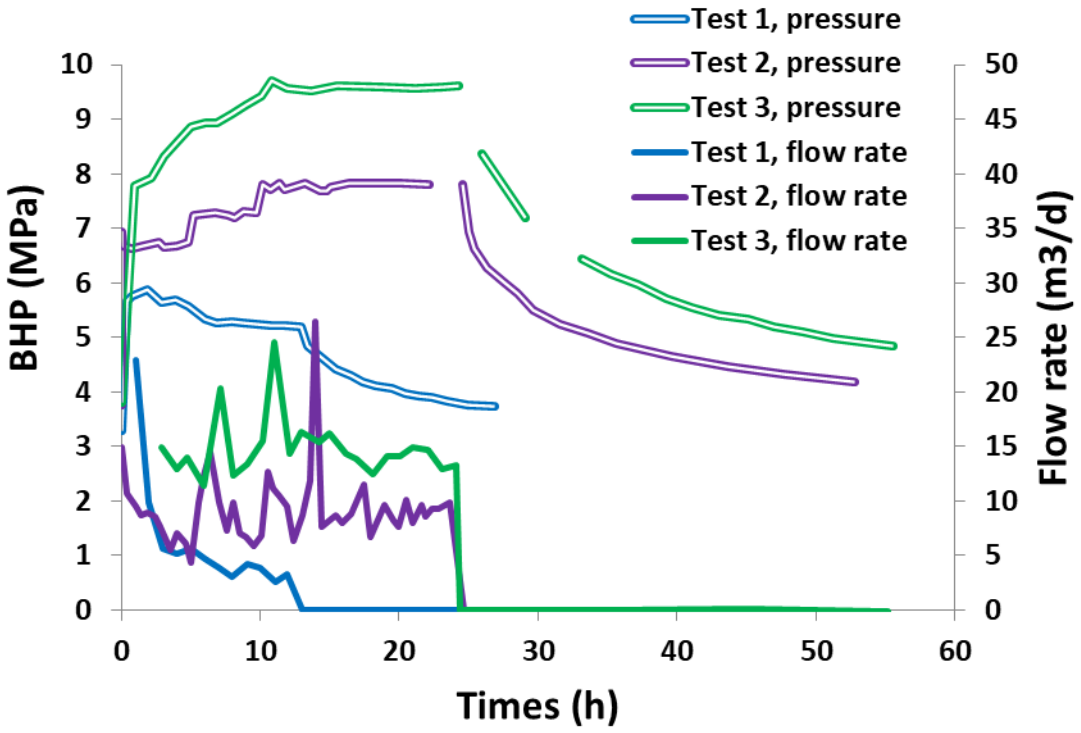

Fig. 10. Results of the well tests in the oil sands in the Burnt Lake project (Xu, 2010).

5.1 Properties of Oil Sands

A bilinear Mohr–Coulomb model with strain hardening/softening was calibrated using a series of triaxial compression tests on Cold Lake oil sands (Wong et al., 1993). The material properties used in the simulation of the base case are provided in Table 1. These properties represent the best estimates based on the limited available data.

Table 1: Summary of the input material properties used in the numerical model

Parameter	Value	Parameter	Value

Maximum principal stress (MPa)[+]	10.35	Tensile strength (MPa)[--]	0.1
Intermediate principal stress (MPa)[+]	8.28	Initial cohesion at LECS (MPa)[*]	0.85
Minimum principal stress (MPa)[+]	7.2	Initial cohesion at HECS (MPa)[*]	4.9
Reservoir pressure (MPa)[+]	3.4	Initial friction angle at LECS (Degree)[**]	21.28
Initial water saturation (%)[+]	30	Initial friction angle at HECS (Degree)[***]	3.45
Elastic modulus (MPa)[++]	Variable	Initial dilation angle at LECS (Degree)[**]	25
Poisson's ratio[++]	Variable	Initial dilation angle at HECS (Degree)[***]	−24.5
Absolute permeability (md)[--]	300	Porosity[---]	34
B_h and B_H[-]	2 and 5		

+ Xu (2010), ++ Assessed from laboratory experiments on Cold Lake oil sands performed by Wong et al. (1993), - Bh and BH are minimum and maximum shear permeability enhancement rates in the Touhidi-Baghini model (Eq. 6), found by sensitivity analysis and history matching, -- From calibrations against experimental data for McMurray oil sands by Touhidi-Baghini (1998), --- Assumed, * calculated from laboratory experiments on Cold Lake oil sands performed by Wong et al. (1993), ** At Low Effective Confining Stress (LECS); calculated from triaxial data for Cold Lake oil sands (Clearwater formation) performed by Wong et al. (1993), *** At High Effective Confining Stress (HECS); calculated from triaxial data for Cold Lake oil sands (Clearwater formation) performed by Wong et al. (1993)

5.2 Model and Grid Sizes

The plane-strain condition was assumed because no formation pressurization is expected due to the relatively short duration of the injection through a vertical wellbore in a 25 m pay zone. The stresses and strains are uniform along the vertical axis, and the displacement in the vertical direction can be ignored. Therefore, a 2D plane-strain model is employed in the pay zone mid-section, and it is expanded in the horizontal direction. Half of the reservoir is modeled due to the symmetry of the reservoir.

Due to the symmetry, the model is composed of a wellbore with a 500 m by 250 m geometry. The plane-strain geomechanical model includes a uniform 1-by-1-m^2 mesh in the vicinity of the injection point and the mesh-size transitions into a coarser grid as the distance from the injection point increases and as the far-field boundaries of the model become closer (Fig. 11).

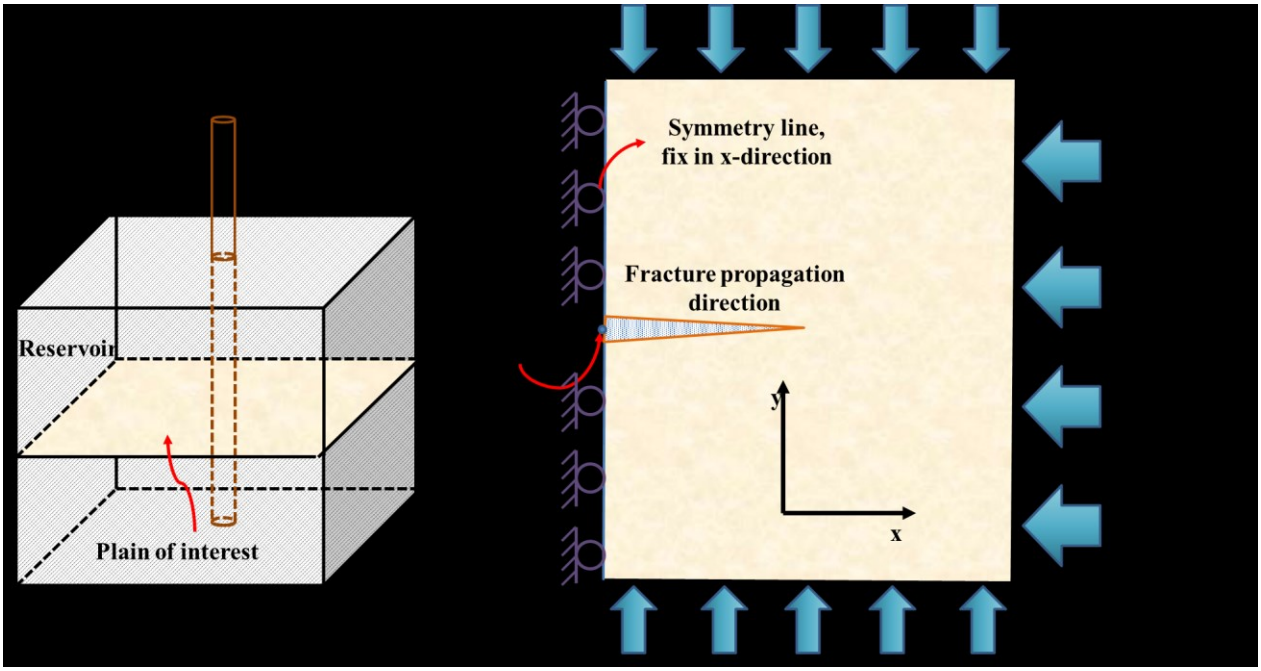

Fig. 11. Geometry and boundary conditions of the model.

5.3 Initial and Boundary Conditions

As shown in Fig. 11, a maximum horizontal stress of 8.28 MPa is applied to the right boundary, whereas a minimum horizontal stress of 7.2 MPa is applied on the top and bottom boundaries. A normal faulting regime is considered with a vertical stress of 10.35 MPa and an initial reservoir pressure of 3.3 MPa. These parameters are used in the geomechanical module.

For flow simulation, the middle of the left boundary is selected as the injection point. Except for the injection point, the remainder of the left boundary is considered to be a no-flow boundary, whereas constant pressure boundaries were assigned to all other boundaries with a pressure equal to the initial reservoir pressure.

5.4 Numerical Model Results

The numerical simulation results were compared to those of the actual well tests. The modeling results are shown in Fig. 12. The numerical simulation indicated that no tensile hydraulic fractures occurred during the three well tests. Similar findings were reported by Xu (2010) in his 3D numerical simulations of these tests. In Xu's paper, he showed that plastic deformations (Test 1) or shear dilative strains (Tests 2 and 3) took place during the well tests. In the current study, the same results were found wherein hydraulically induced dilated zones were observed in the oil sands in Wells 2 and 3.

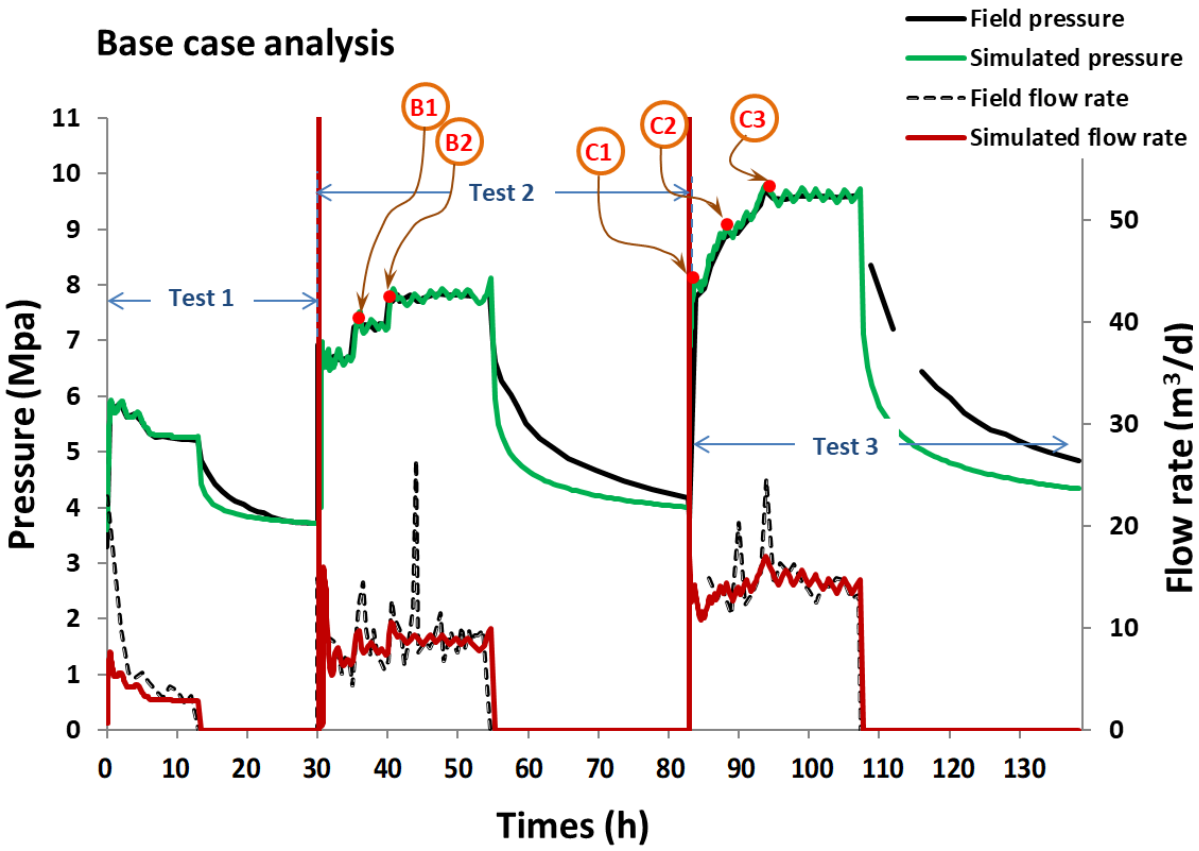

Fig. 12. Simulation results.

5.5 Sensitivity Analysis

A series of analyses were conducted to evaluate the sensitivity of the mesh size on tensile fracture. In addition, further sensitivity analyses were performed with respect to the flow and geomechanical parameters including the apparent tensile strength and cohesion of the oil sands; magnitude of the minimum and maximum principal stresses; absolute permeability and elastic modulus of the oil sands; ramp-up time; and shear-induced permeability changes (*B* parameter).

5.5.1 Effects of the Mesh Size

Three different mesh sizes (2 m × 2 m, 1 m × 1 m, and 0.5 m × 0.5 m) were examined to assess the mesh sensitivity on the modeling results. Figure 13 shows the results of three nominated mesh sizes. A larger element size (2 m × 2 m) resulted in a higher fracturing pressure and a significantly shorter fracture. It also demonstrated a more unstable growth of the length of the fracture. The results appear to converge as the element size is refined to 1 m × 1 m and 0.5 m × 0.5 m. The smaller mesh size demonstrated a smoother fracture growth at the early stages of

injection. Because the smaller mesh is extremely time consuming in terms of the solution time (nearly 120 h were required on a 2.7 GHz CPU Intel i7 PC, 9 GB RAM), a 1 m × 1 m mesh was used for the base case model for the remaining analyses.

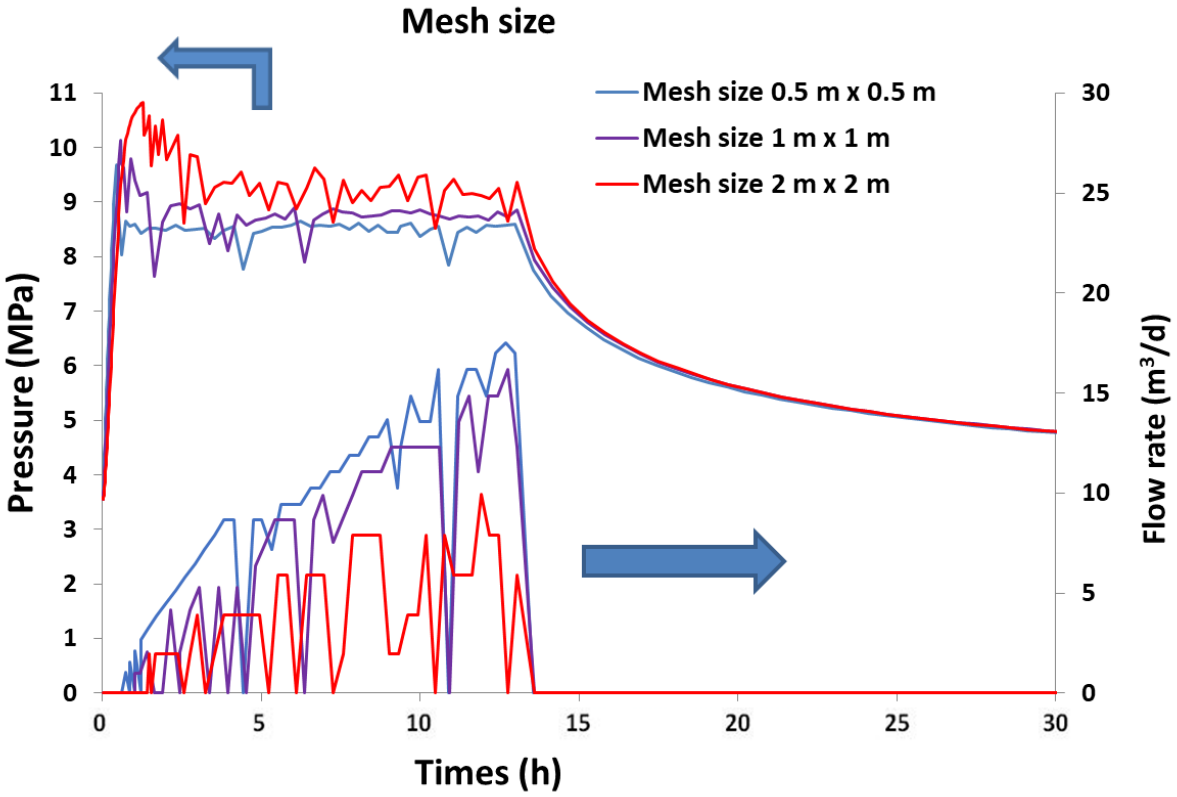

Fig. 13. Impact of the mesh size on the fracture pressure and length.

5.5.2 Effects of the Apparent Tensile Strength

Because different values for the tensile strengths of oil sands have been reported in literature, a sensitivity analysis was performed to evaluate the impact of the tensile strength on the response of the reservoir to fracturing. In addition to the base case (with a tensile strength of 100 kPa), two different tensile strengths of 0.5 kPa and 1.0 MPa were used in the simulations.

Figure 14 illustrates the impact of the tensile strength on the fracturing response of the reservoir, showing that a shorter fracture and slightly larger fracture propagation pressure were observed at higher tensile strengths. The difference in the fracture lengths with tensile strengths of 0.1 and 1.0 MPa was approximately 5 m after 13 h of injection. The difference in the injection pressure, however, was small (almost 0.4 MPa) between these two cases. A lower pressure corresponds to a smaller tensile strength. While the breakdown pressures for the cases with tensile strengths of

0.1 MPa and 0.5 MPa showed little difference, the difference between the cases with tensile strengths of 0.5 MPa and 1.0 MPa was more noticeable. In addition, fewer fracture-length fluctuations were observed in the low tensile-strength case, whereas the fracture length of the case with a larger tensile strength included more closure and opening cycles. This is because the pressure drop in the larger tensile strength case is more significant than in the other cases.

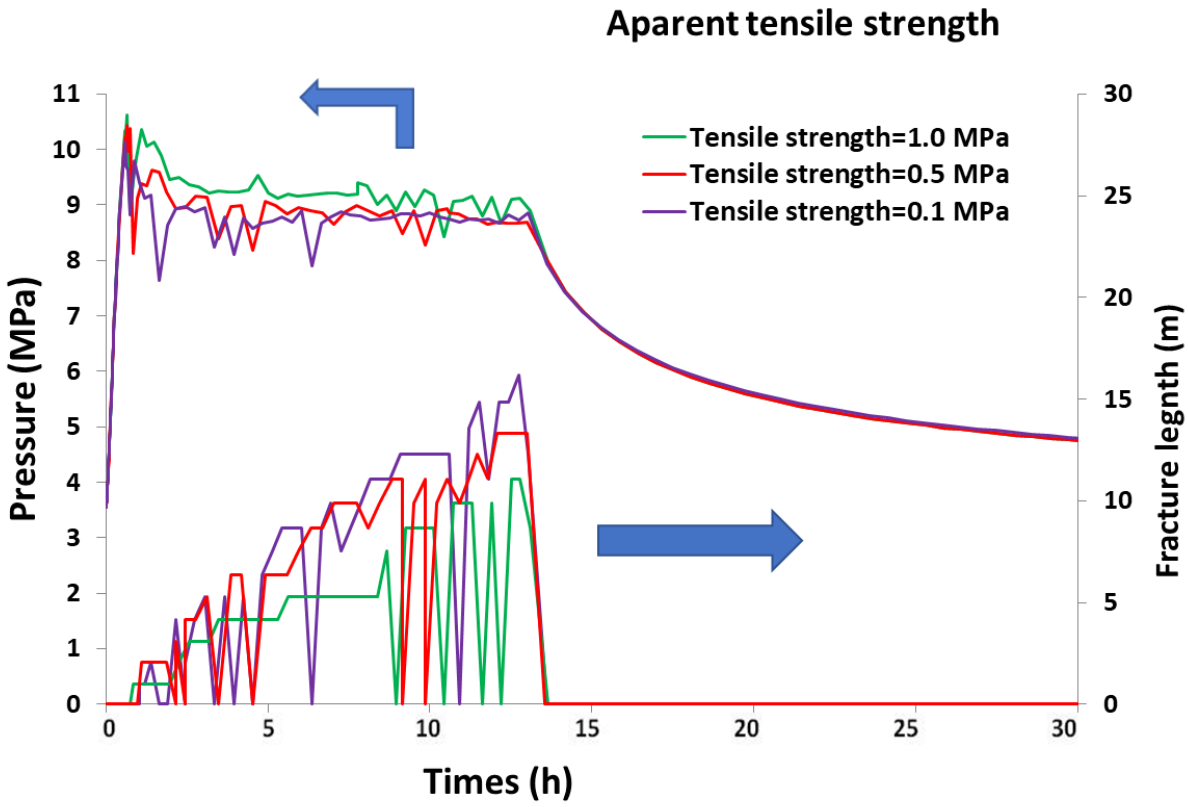

Fig. 14. Sensitivity analysis with respect to the tensile strength of the oil sands.

5.5.3 Effects of the Minimum Principal Stress

A sensitivity study was also conducted with respect to the magnitude of the minimum principal stress. This parameter is believed to directly control the breakdown and propagation pressures. Two minimum principal stresses of 6.7 and 7.7 MPa were considered and compared to the base case. The results are plotted in Fig. 15.

This figure shows that the magnitude of the minimum principal stress has a large impact on the fracturing pressure. Breakdown pressures of 9.35, 10.1, and 11 MPa were found at the minimum stress magnitudes of 6.7, 7.2, and 7.7 MPa, respectively. By increasing the minimum stress in 0.5 MPa increments (6.7, 7.2, and 7.7 MPa), an increase of 0.75 and 0.9 MPa is observed in the

break down pressure, compared to the base case. The propagation pressures of the three cases were 9.6, 8.8, and 8.0 MPa from the larger to smaller minimum stresses, respectively (i.e., 0.8 MPa increments of the propagation pressure were observed for 0.5 MPa increments of the minimum stress). A smaller minimum principal stress therefore results in a longer fracture.

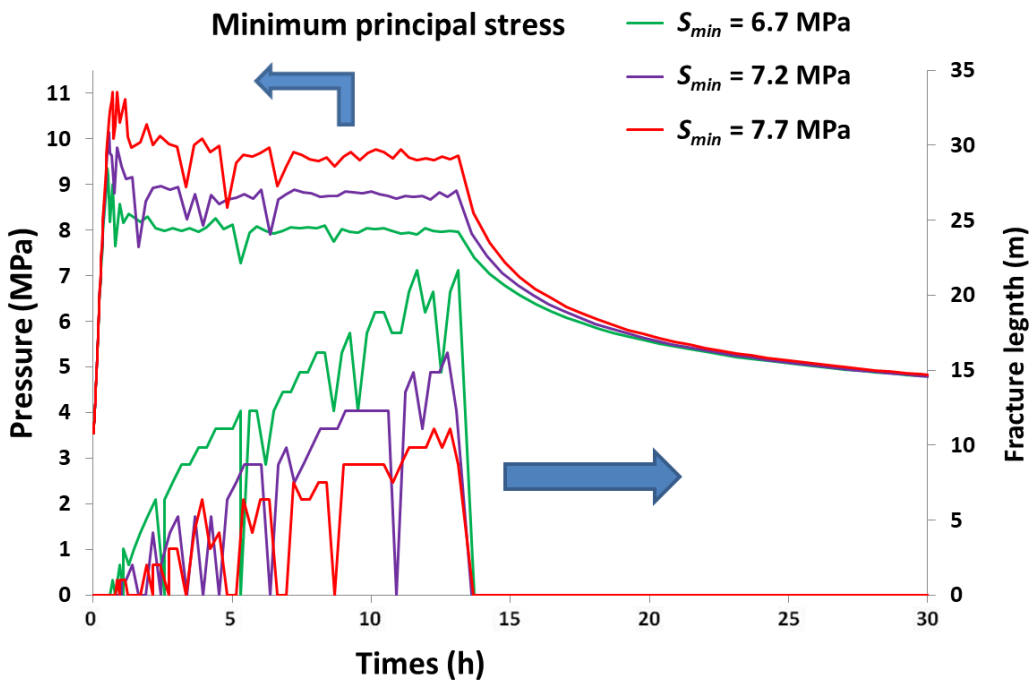

Fig. 15. Impact of the magnitude of the minimum principal stress.

5.5.4 Effects of the Maximum Principal Stress

The influence of the magnitude of the maximum principal stress on the initiation and propagation pressures was also studied. Three maximum principal stresses of 9.85, 10.35 (the base case), and 10.85 MPa were considered.

As plotted in Fig. 16, the three cases show similar breakdown pressures within a difference of 0.25 MPa. The case with the largest maximum principal stress shows the highest propagation pressure. This may be attributed to a higher shear stress and therefore a higher susceptibility to shear yielding and dilation, resulting in higher compressive stresses in the direction of the minimum stress. For the same reason, smaller maximum principal stresses result in a longer fracture. More shearing enhances the permeability of the reservoir, which in turn increases the leak-off and reduces the fracture length. Additionally, high leak-off and high total stress values result in a high fracturing pressure and short fracture length.

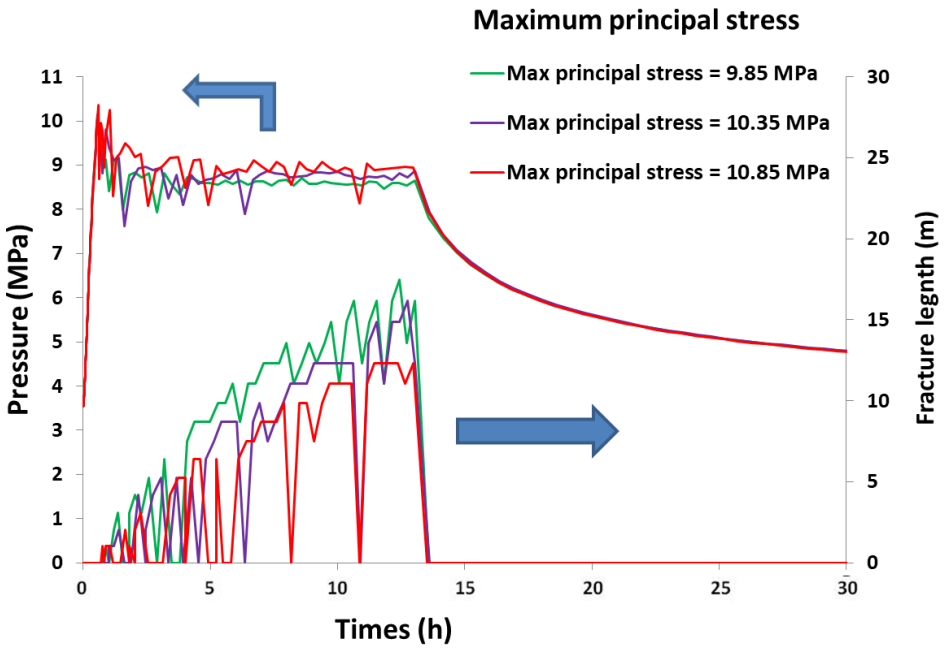

Fig. 16. Impact of the magnitude of the maximum principal stress.

The results showed that for the same reservoir and geomechanical conditions, a larger deviatoric stress state resulted in a larger propagation pressure and a shorter fracture length.

5.5.5 Effects of Cohesion

The amount of cohesion influences the shear strength of the reservoir sand, which affects the fluid leak-off due to the shear-induced permeability, thereby impacting the fracturing pressure and length. To examine the influence of the cohesion on the fracturing response of the reservoir, four initial cohesion values of 0.085, 0.425, 0.85 (the base case), and 1.7 MPa were considered. The same ratio (i.e., the cohesion of the model with respect to the base-case cohesion) was maintained during strain hardening and softening of the material. Figure 17 shows the effects of cohesion on the fracturing pressure.

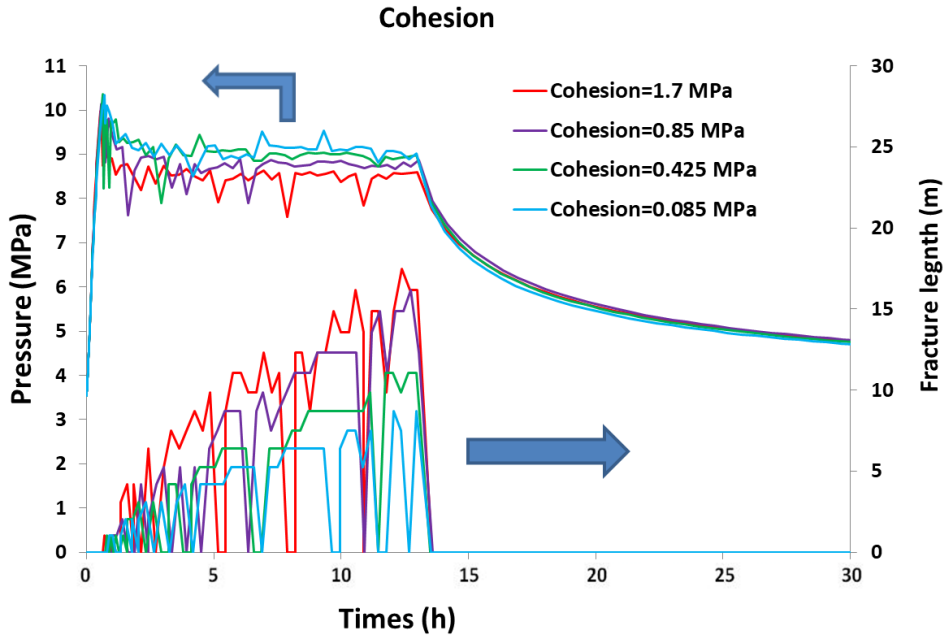

Fig. 17. The influence of cohesion on the fracturing pressure.

As expected, higher cohesion resulted in a longer fracture length but lower fracturing pressure. Cohesions of 0.085, 0.425, 0.85 (the base case), and 1.7 MPa led to breakdown pressures of 10.36, 10.34, 10.10, and 9.97 MPa, respectively. Additionally, the fracture propagation pressures were found to be 9.1, 8.95, 8.75, and 8.55 MPa, respectively.

The results show that cohesion significantly affects the fracture length. Longer fractures are obtained for higher cohesions due to the occurrence of less shearing and lower leak-off rates from the fracture walls. The low-cohesion case (0.085 MPa) demonstrated many cycles of fracture closure and pressure increases that re-opened the fracture during the injection period. This phenomenon can be attributed to the extensive shearing and dilation around the fracture walls and wellbore. Shearing results in dilation, which increases the magnitude of the local minimum principal stresses. Therefore, it tends to close the fracture. To re-open the fracture, higher pressures are required.

5.5.6 Effects of the Shear Permeability Evolution Rate (*B* parameter).

The *B* parameter in the Touhidi-Baghini shear permeability model (Touhidi-Baghini, 1998) influences the extent of permeability enhancement with the accumulation of shear deformation. It thereby affects the leak-off rate from the fracture walls and impacts both the fracturing pressure and length. The *B* parameter should therefore be evaluated via permeability

measurements during triaxial compression tests. These data sets are not available for the reservoir being studied, and the B value is assumed based on the recommendations of Touhidi-Baghini. To understand the effects of the B parameter on the fracturing response, a sensitivity analysis was performed.

Three B_h values of 1, 2 (the base case), and 3 were considered, whereas the B_H/B_h ratio was maintained equal to 2. Figure 18 shows the effects of B on the breakdown and propagation pressures. All three cases show basically the same breakdown and propagation pressures. However, a higher B value shows a slightly shorter fracture, which is expected due to the increased water leak-off from the fracture walls. Furthermore, fewer fluctuations in the fracture length were observed for smaller B values, especially at the early injection stages. This may be a function of the smaller permeability at the shear zone on the fracture walls, which results in less leak-off from the walls. A smaller leak-off leads to decreased shearing, as well as decreased variation in the stresses and pore pressures near the hydraulic fracture, all of which contribute to more stable fracture growth.

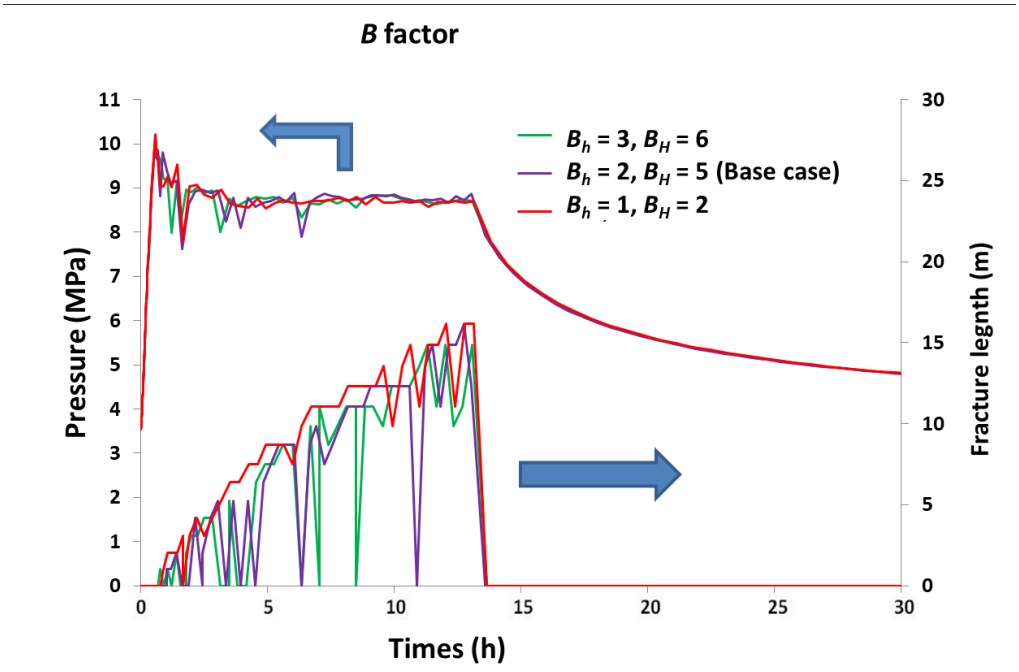

Fig. 18. Influence of the shear permeability evolution rate (B parameter).

5.5.7 Effects of the Ramp-Up Time

A quicker pressure ramp-up results in decreased leak-off, which affects the fracturing response of the reservoir. To investigate this effect, four different ramp-up times of 16.5, 33 (base case),

66, and 100 min were considered, as shown in Fig. 19.

This figure shows that fracture initiation is delayed for the case with a slower ramp-up than the base case. However, the breakdown pressures and propagation pressures do not vary to large extent. A faster injection rate leads to earlier fracture initiation and a slightly longer fracture.

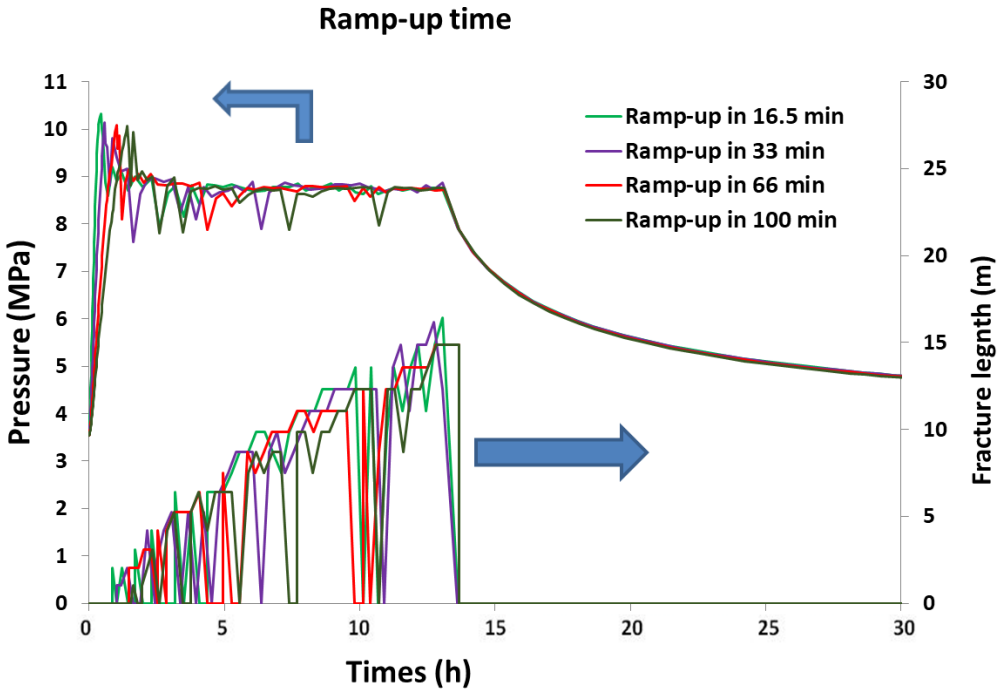

Fig. 19. Sensitivity analysis with respect to the ramp-up time.

5.6 Discussion of the Results of the Sensitivity Analyses

A sensitivity study of important geomechanical parameters was performed, including the apparent tensile strength and cohesion of the oil sands; magnitude of the minimum and maximum principal stresses; absolute permeability and elastic modulus of the oil sands; ramp-up time; and shear-induced permeability changes. The impacts and importance of these variables on the simulation results were evaluated. Additionally, an optimized mesh size was determined in terms of the convergence and simulation time.

In previous studies, different values of the oil sand tensile strengths have been used. Based on the sensitivity analysis conducted in this study, the tensile strength has a noticeable effect on the fracture geometry (length) and, to a lesser extent, on the breakdown pressure. Therefore, numerical simulations may only be valid when the tensile strength of the oil sand has accurately been predetermined. The sensitivity results of the maximum and minimum principal stresses

indicate that both the fracture length and breakdown pressure are influenced by alterations in the stress magnitudes. The estimation of these stresses is challenging, and it involves errors and uncertainties. Therefore, the simulation results might be affected via the estimation of these stresses. It was also observed that the cohesion parameter has a significant impact on the fracture length, resulting in longer fractures at higher values of cohesion. The simulations conducted in this paper are focused on oil sands, which generally possess lower values of cohesion compared to competent sandstones. Therefore, shorter fracture lengths should be expected to form in oil sands. The fracture length was also observed to be highly sensitive to the elastic modulus, such that longer fractures are formed with higher elastic moduli. The use of increased B values produced slightly shorter fractures, which is expected due to the increased leak-off from the fracture walls. Based on these results, it was shown that a lower absolute permeability contributes to a lower breakdown pressure and a longer fracture length. A high-pressure ramp-up time is associated with a relatively lower leak-off rate, which results in the formation of longer fractures.

According to the aforementioned results of the sensitivity studies, the geomechanical and physical properties of the media could potentially alter the numerical simulation results significantly. These results may also be affected by the variation in the operational parameters of the pressure ramp-up time and the B parameter, but to a lesser extent. Therefore, it is essential to have reliable measurements of these parameters to obtain realistic results from numerical simulations.

6 Conclusion

The smeared fracture approach was employed to develop a hydraulic fracture model. The modeling scheme was verified using previously published numerical results for tensile fractures. The results indicate that the smeared fracture approach can appropriately simulate the tensile hydraulic fracturing process.

The fracture energy regularization method was applied to ensure that the energy dissipated during fracture propagation was independent of the mesh size. However, some mesh dependency was still observed, and there are several possible explanations for this phenomenon: the requirement for different mesh sizes to have different volumes of fluid to increase the pressure to the fracturing level; the finite difference scheme employed in FLAC; and the truncation error in the calculations. An examination of the fracture energy regularization method showed that when it is used in the numerical continuum model, the method could reduce the mesh dependency of the computations.

Three well tests in a cold oil sand reservoir were simulated in this study using the developed

smeared hydraulic fracture model. This model has the ability to simulate the hydraulic fracture initiation and propagation without the need to predefine the fracture orientation or location.

A comprehensive sensitivity analysis of the geomechanical and operational parameters was performed to determine the influence of each variable on the numerical simulation results. It was observed that the fracture response of the reservoir in terms of the fracture length and breakdown pressure is highly sensitive to variations in the mechanical and physical parameters of the rock. These parameters include the tensile strength, elastic modulus, absolute permeability, cohesion, and maximum and minimum principal stresses. Additionally, the B parameter and operational parameter of the pressure ramp-up rate were also observed to affect the simulation results, but to a lesser extent than the aforementioned parameters. Moreover, differences between the geomechanical and physical properties of unconsolidated oil sands and competent sandstones result in very different hydraulic fracturing simulation results for these two cases.

The results of the numerical model and approach employed in this study agree with those of the well tests and 3D simulation conducted by Xu (2010). The well test data indicate the occurrence of no tensile fractures and the formation of hydraulically induced dilated zones in the oil sands.

Conflict of interest

The authors certify that they have no conflict of interest or affiliations with any organization or entity with any financial interest in the subject matter or materials discussed in this manuscript.

Acknowledgment

The authors would like to acknowledge the research funding for this study provided by NSERC through Grant No. CRDPJ 387606-09.

References

Anderson, T. L. (1991). Fracture Mechanics: Fundamentals and Applications. CRC Press, Boca Raton.

Barenblatt, G. I. (1962). The Mathematical Theory of Equilibrium Cracks in Brittle Fracture. Advances in Applied Mechanics 7, 55-129.

Bažant, Z. (1984). Microplane Model for Strain-Controlled Inelastic Behaviour. Page 15 in Mechanics of Engineering Material. John Wiley & Sons.

Bažant, Z. and Oh, B. (1983). Crack band theory for fracture of concrete. Materials and Structures 16(3), 155-177.

Bažant, Z. P., Lin, F.-B. and Lippmann, H. (1993). Fracture energy release and size effect in borehole breakout. International Journal for Numerical and Analytical Methods in Geomechanics 17, 1-14.

Bésuelle, P., Desrues, J. and Raynaud, S. (2000). Experimental characterisation of the localisation phenomenon inside a Vosges sandstone in a triaxial cell. International Journal of Rock Mechanics and Mining Sciences, 37(8), 1223-1237.

Bohloli, B. and de Pater, C. J. (2006). Experimental study on hydraulic fracturing of soft rocks: Influence of fluid rheology and confining stress. Journal of Petroleum Science and Engineering 53(1/2), 1-12.

Chang, H. (2004). Hydraulic Fracturing in Particulate Material. PhD Thesis. Georgia Institute of Technology, Georgia, Atlanta.

Chin, L. Y. and Montgomery, C. T. (2004). A Numerical Model for Simulating Solid Waste Injection in Soft Rock Reservoirs. SPE Annual Technical Conference and Exhibition, Houston, Texas. 90507.

Cook, B. K., Lee, M. Y., DiGiovanni, A. A., Bronowski, D. R., Perkins, E. D. and Williams, J. R. (2004). Discrete Element Modeling Applied to Laboratory Simulation of Near-Wellbore Mechanics. International Journal of Geomechanics 4(1), 19-27.

Crook, T., Willson, S., Yu, J. G. and Owen, R. (2003). Computational modelling of the localized deformation associated with borehole breakout in quasi-brittle materials. Journal of Petroleum Science and Engineering 38(3/4), 177-186.

Daneshy, A. A. (2003. Off-Balance Growth: A New Concept in Hydraulic Fracturing. SPE Journal of Petroleum Technology, 55(4), 78-85.

Daneshy, A. A. (2011). Hydraulic Fracturing of Horizontal Wells: Issues and Insights. SPE Hydraulic Fracturing Technology Conference, 24-26 January, The Woodlands, Texas, USA.

de Borst, R. and Nauta, P. (1985). Non-Orthogonal Cracks in a Smeared Finite Element Model. Engineering Computations 2(1), 35-46.

de Pater, C. J. and Dong, Y. (2007). Experimental Study of Hydraulic Fracturing in Sand as a Function of Stress and Fluid Rheology. Page 10 SPE Hydraulic Fracturing Technology Conference. Society of Petroleum Engineers, College Station, Texas USA. SPE 63233.

Desai, C. S. (2001). Mechanics of materials and interfaces: the disturbed state concept. CRC Press.

Di Lullo, G., Curtis, J. and Gomez, J. (2004). A Fresh Look at Stimulating Unconsolidated Sands with Proppant-Laden Fluids. Page 5 SPE Annual Technical Conference and Exhibition. Society of Petroleum Engineers, Houston, Texas. 90813-MS.

Duan, K., Kwok, C.Y., Wu, W. and Jing, L. (2018). DEM modeling of hydraulic fracturing in permeable rock: influence of viscosity, injection rate and in situ states. Acta Geotechnica, 13(5), 1187-1202.

Gidley, J. L., Holditch, S. A., Nierode, D. E. and Veatch, R. W., Jr. (1989). Recent Advances in Hydraulic Fracturing. Society of Petroleum Engineers, Dallas, Texas.

Gil, I. (2005. Hydraulic fracturing of poorly consolidated formations: Considerations on rock properties and failure mechanisms. PhD Thesis. University of Oklahoma, Oklahoma.

Gil, I. and Roegiers, J. (2006). The Effect of Fluid Leakoff on Rock Failure Mechanisms During Frac-Pack Treatments. Page 7 International Symposium and Exhibition on Formation Damage Control. Society of Petroleum Engineers, Lafayette, Louisiana U.S.A. 98170.

Golovin, E., Jasarevic, H., Chudnovsky, A., Dudley, J. W. and Wong, G. K. (2010). Observation and Characterization of Hydraulic Fracture in Cohesionless Sand. Page 9 44th U.S. Rock Mechanics Symposium and 5th U.S.-Canada Rock Mechanics Symposium. American Rock Mechanics Association, Salt Lake City, Utah. ARMA10-359.

Hagoort, J., Weatherill, B. D. and Settari, A. (1980). Modeling the Propagation of Waterflood-Induced Hydraulic Fractures. SPE Journal, 20(4), 293-303. 7412.

Howard, G. C. and Fast, C. R. (1970. Hydraulic Fracturing. Millet the Printer, Dallas TX.

Hu, D. W., Zhou, H., Zhang, F. and Shao, J. F. (2010). Evolution of poroelastic properties and permeability in damaged sandstone. International Journal of Rock Mechanics and Mining Sciences 47(6), 962-973.

Huang, H., Zhang, F., Callahan and Ayoub, J. (2011). Fluid Injection Experiments in Two-dimensional Porous Media. Page 8 SPE Hydraulic Fracturing Technology Conference. Society of Petroleum Engineers, The Woodlands, Texas, USA. 140502-MS.

Itasca Consulting Group Inc. (2011). FLAC Fast Lagrangian Analysis of Continua: User's Guide, Minneapolis, Minnesota.

Jafarpour, M., Rahmati, H., Azadbakht, S., Nouri, A., Chan, D. and Vaziri, H. (2012). Determination of Mobilized Strength Properties of Degrading Sandstone. Soils and Foundations 52(6), 658-667.

Jasarevic, H., Golovin, E., Chudnovsky, A., Dudley, J. W. and Wong, G. K. (2010). Observation and Modeling of Hydraulic Fracture Initiation in Cohesionless Sand. Page 9 44th U.S. Rock Mechanics Symposium and 5th U.S.-Canada Rock Mechanics Symposium. American Rock Mechanics Association, Salt Lake City, Utah. ARMA 10-360.

Ji, L. (2008). Modeling Hydraulic Fracturing Fully Coupled with Reservoir and Geomechanical Simulation. Ph.D. Dissertation. University of Calgary, Calgary, AB.

Ji, L., Settari, A. and Sullivan, R. B. (2006). A New Approach to Hydraulic Fracturing Modeling— Fully Coupled with Geomechanical and Reservoir Simulation. SPE Europec/EAGE Annual Conference and Exhibition Vienna, Austria. 9.

Ji, L., Settari, A. and Sullivan, R. B. (2009). A Novel Hydraulic Fracturing Model Fully Coupled with Geomechanics and Reservoir Simulation. SPE Journal 14(3), 423-430.

Ji, L., Settari, A., Sullivan, R. B. and Orr, D. (2004). Methods for Modeling Dynamic Fractures In Coupled Reservoir And Geomechanics Simulation. Page 9 SPE Annual Technical Conference and Exhibition. SPE, Houston, Texas. 90874-MS.

Khodaverdian, M. and McElfresh, P. (2000). Hydraulic Fracturing Stimulation in Poorly Consolidated Sand: Mechanisms and Consequences. Page 13 SPE Annual Technical Conference and Exhibition. Society of Petroleum Engineers, Dallas, Texas. SPE 63233.

Khodaverdian, M., Sorop, T., Postif, S. and Hoek, P. V. d. (2010). Polymer Flooding in Unconsolidated-Sand Formations: Fracturing and Geomechanical Considerations. SPE Production & Operations 25(2), 211-222.

Klerck, P. A. (2000). The Finite Element Modelling of Discrete Fracture in Quasi-Brittle Materials. PhD Thesis. University of Wales Swansea, Wales UK.

Lian, Z. L., Wang, X. X., Wu1, H. A., Xue1, B., Zhang, J. and Zhang, S. C. (2006). Modeling and Simulation of Hydraulic Fracturing Propagation in Permeable Reservoirs. Key Engineering Materials 324-325, 383-386.

Mahrer, K. D., Aud, W. W. and Hansen, J. T. (1996). Far-Field Hydraulic Fracture Geometry: A Changing Paradigm. SPE Annual Technical Conference and Exhibition, Denver, Colorado. 36441.

McElfresh, P. M., Khodaverdian, M. F. and Baycroft, P. D. (2002). Frac Packing in Soft Formations: Low Efficiency Fluids Exacerbate Formation Damage. Page 12 International Symposium and Exhibition on Formation Damage Control. Society of Petroleum Engineers, Lafayette, Louisiana.

Nagel, N., Gil, I., Sanchez-Nagel, M. and Damjanac, B. (2011). Simulating Hydraulic Fracturing in Real Fractured Rocks - Overcoming the Limits of Pseudo3D Models. SPE Hydraulic Fracturing Technology Conference. Society of Petroleum Engineers, The Woodlands, Texas, USA. SPE-140480-MS.

Nghiem, L. X., Forsyth Jr., P. A. and Behie, A. (1984). A Fully Implicit Hydraulic Fracture Model. SPE Journal of Petroleum Technology, 36(7), 1191-1198.

Nguyen, N.H., Bui, H.H., Nguyen, G.D. and Kodikara, J. (2017). A cohesive damage-plasticity model for DEM and its application for numerical investigation of soft rock fracture properties. International Journal of Plasticity, 98, 175-196.

Nouri, A., Kuru, E. and Vaziri, H. (2009). Elastoplastic Modelling of Sand Production Using Fracture Energy Regularization Method, 48(4), 64-71.

Olson, J. E., Holder, J. and Hosseini, S. M. (2011). Soft Rock Fracturing Geometry and Failure Mode in Lab Experiments. Page 9 SPE Hydraulic Fracturing Technology Conference. SPE, The Woodlands, Texas, USA. SPE 140543.

Onaisi, A., Ochi, J., Mainguy, M. and Souillard, P. A. (2011). Modelling Non-Matrix Flow and Seals Integrity in Soft Sand Reservoirs. SPE European Formation Damage Conference. Society of Petroleum Engineers, Noordwijk, The Netherlands. 144801.

Pak, A. (1997. Numerical Modeling of Hydraulic Fracturing. PhD Thesis. Alberta, Edmonton.

Pak, A. and Chan, D. H. (2004). A Fully Implicit Single-Phase T-H-M Fracture Model for Modelling Hydraulic Fracturing in Oil Sands. Journal of Canadian Petroleum Technology 43(6), 10.

Papanastasiou, P. (1997a). The Influence of Plasticity in Hydraulic Fracturing. International Journal of Fracture 84(1), 61-79.

Papanastasiou, P. C. (1997b). A Coupled Elastoplastic Hydraulic Fracturing Model. International Journal of Rock Mechanics and Mining Sciences 34, 240.e241-240.e215.

Papanastasiou, P. (1999). An efficient algorithm for propagating fluid-driven fractures. Computational Mechanics 24: 258-267.

Pietruszczak, S. and Mróz, Z. (1981). Finite element analysis of deformation of strain-softening materials. International Journal for Numerical Methods in Engineering 17(3), 327-334.

Rege, N. (1996. Computational modeling of granular Materials. Thesis. MIT, Cambridge, Mass.

Roostaei, M., Taghipoor, S., Nouri, A., Fattahpour, V. and Chan, D. (2019). Smeared modeling of hydraulic fracture using partially coupled reservoir and geomechanics simulators. International Journal of Rock Mechanics and Mining Sciences, 113, 99-111.

Settari, A. (1980). Simulation of Hydraulic Fracturing Processes. SPE Journal 20(6), 487-500.

Settari, A. (1988). Modeling of Fracture and Deformation Processes in Oil Sands. Page 14 4th UNITAR/UNDP Conference on Heavy Crude and Tar Sands, Edmonton, AB, Canada. Paper No. 43.

Settari, A., Ito, Y. and Jha, K. N. (1992). Coupling of A Fracture Mechanics Model and A Thermal Reservoir Simulator for Tar Sands. Journal of Canadian Petroleum Technology,31(9), 92-09-02.

Settari, A., Kry, P. R. and Yee, C. T. (1989). Coupling of Fluid Flow and Soil Behaviour to Model Injection Into Uncemented Oil Sands. The Journal of Canadian Petroleum Technology 28(1), 12. 89-01-08.

Settari, A., Puchyr, P. J. and Bachman, R. C. (1990). Partially Decoupled Modeling of Hydraulic Fracturing Processes. SPE Production Engineering, 5(1), 37-44.

Settari, A., Sullivan, R. B. and Bachman, R. C. (2002a). The Modeling of the Effect of Water Blockage and Geomechanics in Waterfracs. SPE Annual Technical Conference and Exhibition, San Antonio, Texas. 77600.

Settari, A., Sullivan, R. B., Walters, D. A. and Wawrzynek, P. A. (2002b). 3-D Analysis and Prediction of Microseismicity in Fracturing by Coupled Geomechanical Modeling. SPE Gas Technology Symposium, Calgary, Alberta, Canada. 75714.

Suidan, M. and Schnobrich, W. C. (1973). Finite Element Analysis of Teinforced Concrete. Journal of the Structural Division, ASCE 99(1), 2109-2122.

Sulem, J., Vardoulakis, I., Papamichos, E., Oulahna, A. and Tronvoll, J. (1999). Elasto-plastic modelling of Red Wildmoor sandstone. Mechanics of Cohesive-frictional Materials 4(3), 215-245.

Taghipoor, S., Roostaei, M., Nouri, A. and Chan, D., (2014). June. A Numerical Investigation of the Hydraulic Fracturing Mechanism in Oil Sands. SPE Heavy Oil Conference-Canada. Society of Petroleum Engineers.

Taghipoor, S., Nouri, A. and Chan, D. (2015). Numerical Modelling of Hydraulic Fracturing in Cohesionless Sand: Validation Against Laboratory Experiments. Journal of Canadian Petroleum Technology, 54(6), 460-474.

Touhidi-Baghini, A. (1998). Absolute Permeability of McMurray Formation oil sands at low confining stresses. PhD Thesis. University of Alberta, Edmonton.

van Dam, D. B., Papanastasiou, P. and Pater, C. J. d. (2000). Impact of Rock Plasticity on Hydraulic Fracture Propagation and Closure. SPE Annual Technical Conference and Exhibition. Copyright (2000, Society of Petroleum Engineers Inc., Dallas, Texas. 63172.

Waite, M. E., Ge, S. and Spetzler, H. (1999). A New Conceptual Model for Fluid Flow in Discrete Fractures: An experimental and numerical study. Journal of Geophysical Research: Solid Earth, 104(B6), 13049-13059.

Wang, Y., Bui, H., Nguyen, G. and Ranjith, P. (2017). A mesh-free continuum based computational approach to modelling rock fracture. Proceedings of the Sixth Biot Conference on Poromechanics, July 9-13, Paris, France. American Society of Civil Engineers.

Wei, H. and Chen, J.S., (2018). A damage particle method for smeared modeling of brittle fracture. International Journal for Multiscale Computational Engineering, 16(4), 303-324.

Weijers, L., Wright, C. A., Sugiyama, H., Sato, K. and Zhigang, L. (2000). Simultaneous Propagation of Multiple Hydraulic Fractures-Evidence, Impact and Modeling Implications. Int. Oil and Gas Conference and Exhibition in China, Beijing, China. 64772.

Weill, L. and Latil, M. (1992). Modelling Hydraulic Fractures in a Finite Difference Reservoir Simulator.in M. A. Christie, F. V. Da Silva, C. L. Farmer, O. Guillon, Z. E. Heinemann, P. Lemonnier, J. M. M. Regtien, and E. Van Spronsen, editors. ECMOR III: 3rd European Conference on the Mathematics of Oil Recovery. Delft University Press, Delf University of Technology, Delf, Netherland.

White, F. M. (2011). Fluid Mechanics. McGraw Hill.

Wolf, H., König, D. and Triantafyllidis, T. (2003). Experimental investigation of shear band patterns in granular material. Journal of Structural Geology 25(8), 1229-1240.

Wong, R. C. K., Barr, W. E. and Kry, P. R. (1993). Stress–Strain Response of Cold Lake Oil Sands. Canadian Geotechnical Journal 30(2), 220-235.

Wu, R. (2006). Some Fundamental Mechanisms of Hydraulic Fracturing. Georgia Institute of Technology, Atlanta.

Xu, B. (2010). Finite Element Simulation of Hydraulic Fracturing in Unconsolidated Sands. Ph.D. Dissertation. University of Calgary, Calgary, AB.

Xu, B. and Wong, R. C. K. (2010). A 3D Finite Element Model for History Matching Hydraulic Fracturing in Unconsolidated Sands Formation. Journal of Canadian Petroleum Technology 49, 58-66.

Xu, B., Yuan, Y. and Wong, R. C. K. (2010). Modeling of the Hydraulic Fractures In Unconsolidated Oil Sands Reservoir. 44th U.S. Rock Mechanics Symposium and 5th U.S.-Canada Rock Mechanics Symposium. American Rock Mechanics Association, Salt Lake City, Utah. 10-123.

Xue, B., Wu, H. a., Wang, X., Lian, Z., Zhang, J. and Zhang, S. (2006). A Three-dimensional Finite Element Model of Hydraulic Progressive Damage. Key Engineering Materials 324/325, 375-378.

Yeung, K. C. (1995). Cold Flow Production of Crude Bitumen at the Burnt Lake Project, Northeastern Alberta. Sixth UNITAR International Conference on Heavy Crude and Tar Sands, Houston, Texas.

Yeung, K. C. and Adamson, M. F. (1991). Burnt Lake Project - Bitumen production form the Cold Lake oil sands deposit without steam. Pages 77-83 44th Canadian Geotechnical Conference. Canadian Geotechnical Society, Calgary, AB, Canada.

Zandi, S., Renard, G., Nauroy, F., Guy, N. and Tijani, M. (2010). Numerical Coupling of Geomechanics and Fluid Flow during Steam Injection in SAGD. Page 10 in SPE 129739 presented at the Improved Oil Recovery Symposium. Society of Petroleum Engineers, Tulsa, Oklahoma, USA.

Zhai, Z. (2006). Fracturing and Fracture Reorientation in Unconsolidated Sands and Sandstones. PhD Thesis. The University of Texas at Austin, Austin.

Zhai, Z. and Sharma, M. M. (2005). A New Approach to Modeling Hydraulic Fractures in Unconsolidated Sands. SPE Annual Technical Conference and Exhibition. Society of Petroleum Engineers, Dallas, Texas. SPE 96246.

Zhang, G. M., Liu, H., Zhang, J., Wu, H. A. and Wang, X. X. (2010). Three-dimensional finite element simulation and parametric study for horizontal well hydraulic fracture. Journal of Petroleum Science and Engineering 72(3/4), 310-317.

Zhou, J., Dong, Y., Pater, C. J. d. and Zitha, P. L. J. (2010). Experimental Study of the Impact of Shear Dilation and Fracture Behavior During Polymer Injection for Heavy Oil Recovery in

Unconsolidated Reservoirs. Page 14 Canadian Unconventional Resources and International Petroleum Conference. SPE, Calgary, AB. SPE 137656-MS.

Zhou, J., Huang, H. and Deo, M., (2016). June. Simulation of hydraulic and natural fracture interaction using a coupled DFN-DEM model. In 50th US rock mechanics/geomechanics symposium. American Rock Mechanics Association.

Zimmerman, R. W. and Bodvarsson, G. S. (1996). Hydraulic conductivity of rock fractures. Transport in Porous Media 23(1), 1-30.

Appendix A: Validation of Touhidi-Baghini's Model for Sandstone

Touhidi-Baghini's shear permeability model (Touhidi-Baghini, 1998) has been proposed for both the isotropic unloading (steam injection) and shearing of oil sands, which are unconsolidated sands. This model should therefore be validated in terms of weakly consolidated or consolidated sandstones. For this purpose, published data (in literature) concerning permeability measurements that were obtained during the triaxial testing of red sandstone (Hu et al., 2010) were used. The measured values of permeability versus the volumetric strains are shown in Fig. A-1. The uniaxial compressive strength (UCS) of this sandstone is approximately 14 MPa. Figure A-1 shows that the permeability of the samples decreases up to a certain level of compaction and then remains nearly constant when dilation starts, followed by an eventual increase. Therefore, the constant portion of this permeability is eliminated from the data (shown by the dashed line in Fig. A-1). The permeability evolution (defined by the ratio of k/k_0) during compaction is shown in Fig. A-2.

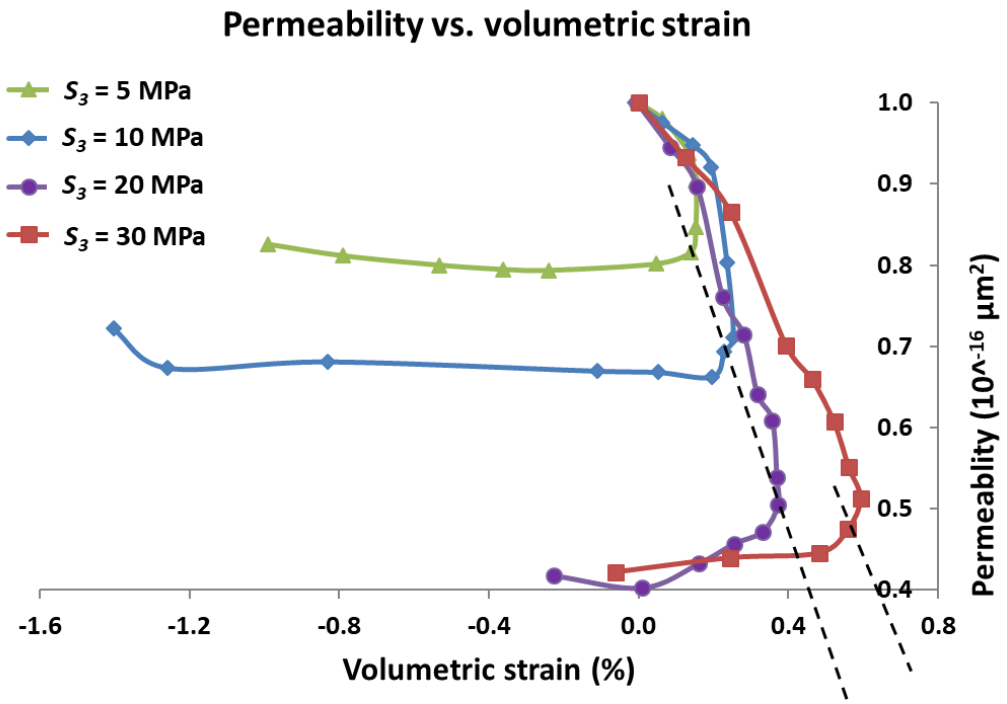

Fig. A-1. Permeability measurements during triaxial tests conducted by Hu et al. (2010)

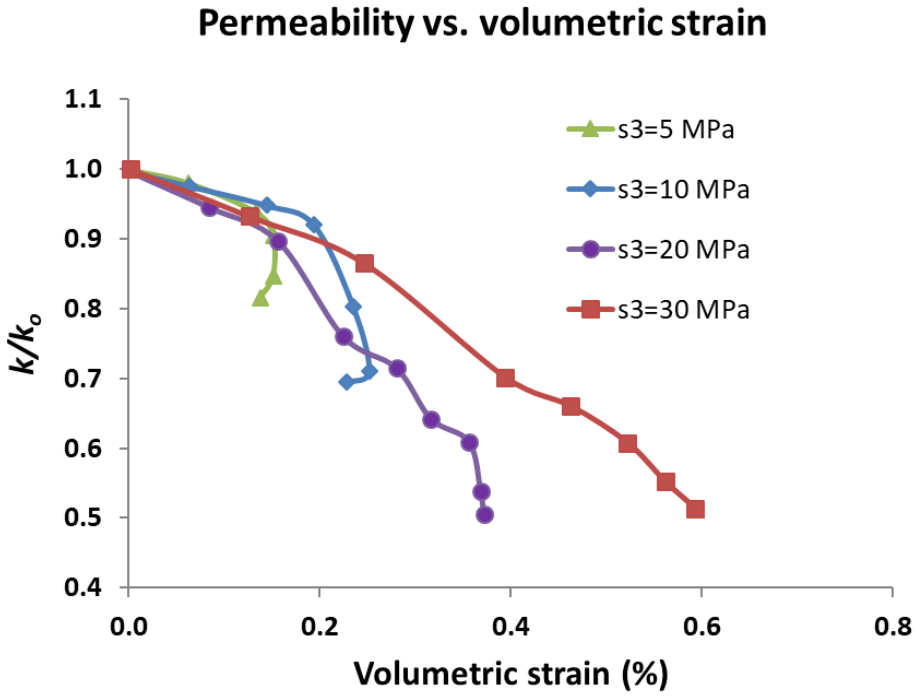

Fig. A-2. Permeability evolution of red sandstone during compaction (Hu et al., 2010)

According to Touhidi-Baghini's shear permeability model (1998), which is shown in Eq. (6), the variation of $\ln(k/k_0)$ and the volumetric strain should demonstrate a linear relationship. Therefore,

the data obtained by Hu et al. (2010) are shown in Fig. A-3 with a linear equation fitted to the data.

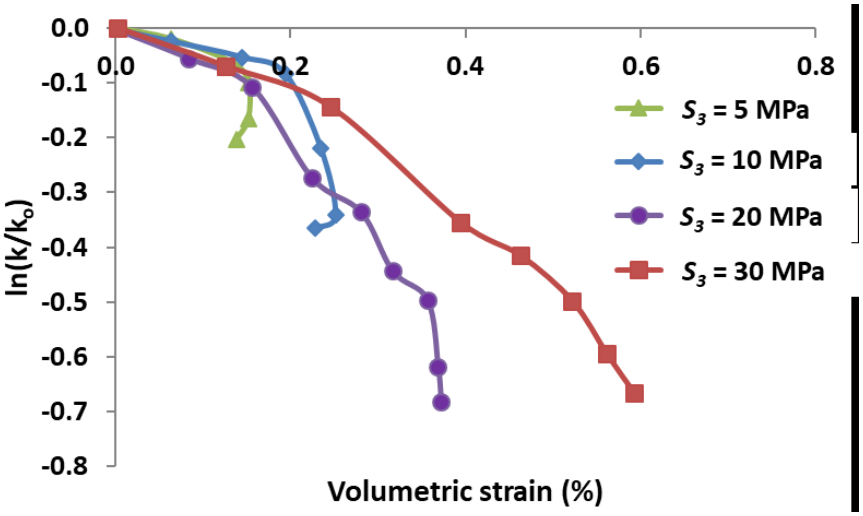

(a) permeability vs. volumetric strain, categorized by minimum in-situ stress

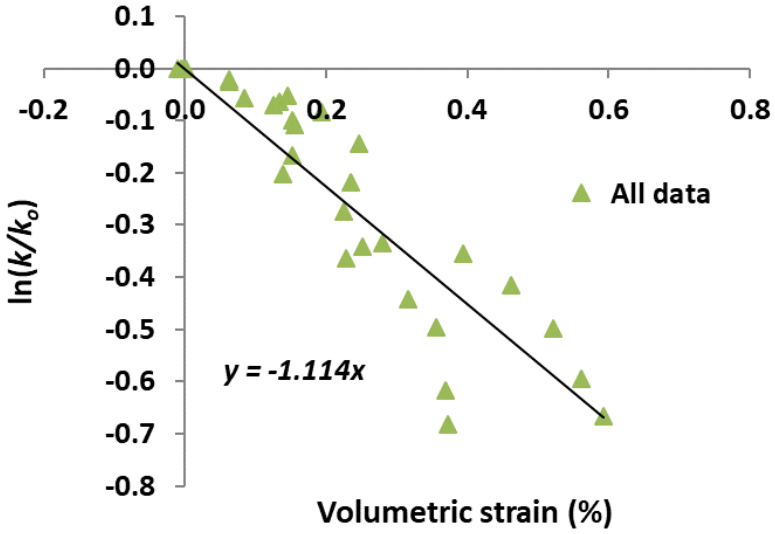

(b) permeability vs. volumetric strain, all data

Fig. A-3. Variation of the permeability ratio of red sandstone during compaction (Hu et al., 2010)

From Fig. A-3, it is demonstrated that the ratio of B/ϕ_0 is equal to −1.114. Knowing that the initial porosity is 0.21, the B factor will be equal to −0.236. Using B = 0.233 in the Touhidi-Baghini's model, the results are shown in Fig. A-4 for all of the experiments.

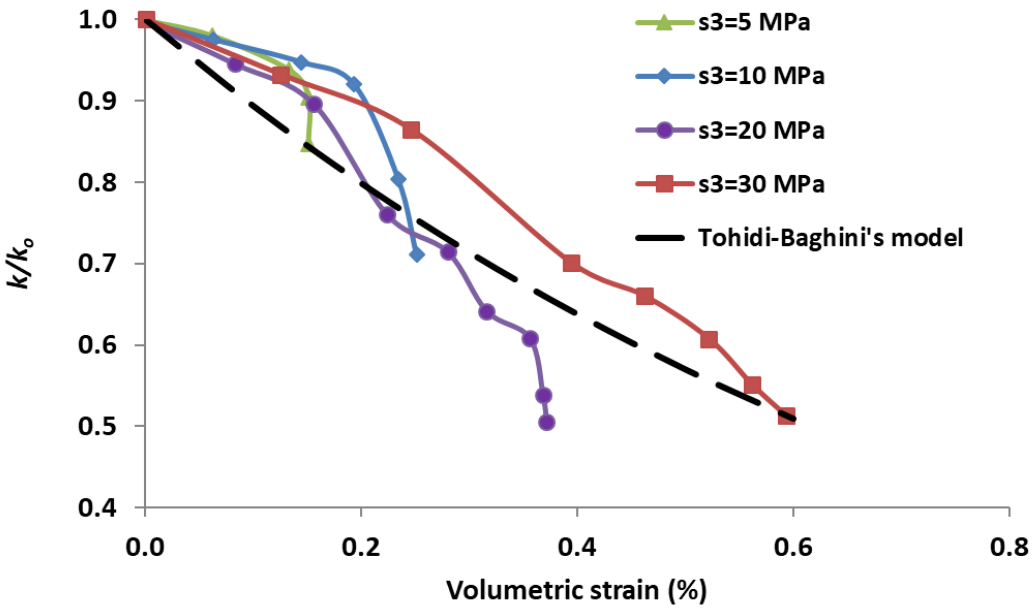

Fig. A-4. Touhidi-Baghini's model with B = 0.233 for all of the experiments performed by Hu (2010)

Figure A-4 shows that the use of Touhidi-Baghini's model reasonably determines the changes in permeability due to volumetric straining for weakly consolidated red sandstone.